Joint Centre for Mesoscale Meteorology, Reading, UK

Collected preprints submitted to the International Symposium on the Life Cycles of Extratropical Cyclones; Bergen, Norway, 27 June - 1 July 1994

JCMM Internal Report No 26

April 1994

Met Office Joint Centre for Mesoscale Meteorology Department of Meteorology
University of Reading PO Box 243 Reading RG6 6BB United Kingdom
Tel: +44 (0)118 378 8425 Fax: +44 (0)118 378 8791
www.metoffice.com

CONTENTS

The Contributions of Ernst Kleinschmidt to Cyclone Research

Alan J Thorpe
Department of Meteorology, University of Reading, England

1 Introduction

The German meteorologist Ernst Kleinschmidt made notable contributions in the field of dynamics and the cyclone problem. The aim of this paper is to present a brief review of these contributions in the context of the modern viewpoint. An expanded version of this paper also including discussion of Kleinschmidt's research on tropical cyclones and ageostrophic windfields can be found in Thorpe 1993.

It should be noted that the references in this paper are divided into numbered contributions from Kleinschmidt and those related papers by other authors. Kleinschmidt's papers will be referred to by their number whereas the others will be referenced in the usual way. In quotations from his papers the original notation and terminology will be preserved. Thus Kleinschmidt uses Z for potential vorticity which is otherwise herein denoted by PV.

Ernst Kleinschmidt was born in Germany on 20 December 1912 the son of an eminent German meteorologist. His undergraduate university education was in mathematics and physics and he obtained a PhD in meteorology under Professor Raethjen's supervision at the University of Hamburg in 1941. Raethjen apparently regarded Kleinschmidt as his best student and gives fulsome praise of his contributions in his book "Dynamik der Zyklonen", published in 1953, putting them alongside those of Rossby. During the war Kleinschmidt was in the Weather Observer Corps of the 2nd Air Fleet Command and travelled extensively. In 1946 he joined the Kaiser Wilhelm Institut für Strömungsforschung (flow research) in Göttingen where he stayed until his death on 4 May 1971. This institute is an illustrious one having been set-up in 1925 with Professor Prandtl as its head. In 1946 Prandtl, aged 71, retired as institute director and in 1948 it was renamed the Max Planck Institut für Strömungsforschung.

Tollmien came to the Max Planck Institut at this time. In the early years after the war Kleinschmidt was an assistant to Prandtl. As research on aerodynamics was forbidden Prandtl decided to pursue research in the more "neutral" field of meteorology.

Kleinschmidt made two scientific visits abroad on invitations from Rossby in 1951 to the University of Stockholm and from Riehl in 1959/60 to the University of Chicago. The former was an attempt by Rossby to bring together scientists from both war camps. Ernst Kleinschmidt's wife Christa, who was also a meteorologist and attended Rossby's conference, recounts that Rossby "....thought of him as an artist because of his imaginative ability". Arnt Eliassen remembers with some regret that Kleinschmidt's lectures in Stockholm were regarded as somewhat queer and

were not taken too seriously.

It is clear that Kleinschmidt's latter years were darkened by depression and loneliness not least because of the adverse reaction to his research of that later period on ageostrophic wind-fields. Professor Tollmien did not allow Kleinshmidt to pursue this work contrary, as it was, to the accepted view.

2 Symmetric instability

The first two papers of Kleinschmidt (1 and 2) describe his PhD thesis work on dynamical instability. This topic was one which was of considerable interest at that time having been considered by Helmholtz (1888) and Solberg (1928) as an explanation for cyclone development; the latter paper was not referenced by Kleinschmidt. The use of the term dynamical is to distinguish this from static instability. At that time baroclinic instability had not been discovered but following its introduction the term symmetric, rather than dynamical, is now used. This is because the theoretical description of dynamical instability is of a two-dimensional baroclinic type mode; with other instabilities being discovered the term dynamical is clearly too broad.

A simplified stability analysis is presented in (1) giving the criterion for this two-dimensional instability to be that the isentropic absolute vorticity should be negative. The analysis is different from that of Helmholtz and more general in applying to a continuously varying fluid rather than only to a 2-fluid layer model. It appears to be a simplified form of the parcel model introduced by Solberg (1928). A discussion follows about the possible geographical variations in the instability, the extension to saturated flow by using θ_e surfaces, and the possibility of a moist neutral condition applying at fronts. Also the mechanism of destabilizing the atmosphere is discussed. One is left with the feeling that this is a theory waiting for a proper application to the atmosphere by making a detailed synoptic data analysis. This was to come after the war when Kleinschmidt began work in Prandtl's laboratory. The complete mathematical description of moist or conditional symmetric instability awaited the work of Bennetts and Hoskins (1979), although in the intervening years several authors (including most notably Sawyer) considered the topic of some importance in describing frontal structure.

3 Tropopause cyclones

In a three part paper entitled "On the structure and origin of cyclones" (3, 4 and 5) Kleinschmidt explored how PV concepts could be used to construct a paradigm concerning extratropical cyclones. It should be remembered that at that time, following the Bergen school's identification of cyclone families on the so-called polar front, the hunt was on for a convincing theoretical explanation for the formation of such wave or frontal cyclones. Baroclinic wave theory in the form of a linear normal mode instability had been described in publications by Charney (1947) and Eady (1949). These papers are not referred to by Kleinschmidt so we do not know whether he was unaware of their existence (probably unlikely) or felt them to be irrelevant to the approach he was taking. The latter view is defensible as Kleinschmidt's approach has similarities to that of the Norwegians in developing ideas from synoptic case studies rather than that of the mathematical fluid dynamics approach of Charney and Eady. Furthermore his model was inherently finite amplitude in nature in that it considers the processes maintaining a cyclone rather than conceiving of a, hypothetical, basic flow which might exhibit growth of infinitesimal perturbations.

In part 1 (3) Kleinschmidt looks at a cyclone, which to modern eyes is not a very remarkable one, which developed over a 12 hr period on 6 March 1943 to give more precipitation than seemed likely from its previous history. From routine radiosounding data he notes the existence of ".... a lentiform mass, differing from the surrounding masses by a very different gradient of θ, settled between the troposphere and stratosphere to the west of the ground cyclone. This body or 'Höhenkörper' is the primary object of our investigation". We reproduce his figures 2 and 4 as our figure 1.

The Höhenkörper can be followed for 36 hr and Kleinschmidt goes on to state that "There is no doubt that the body was the cause of the further development of the low ...It drifts along from the north-west, almost catches up with the depression but then turns off southwards to the Mediterranean, while the low continue on its way

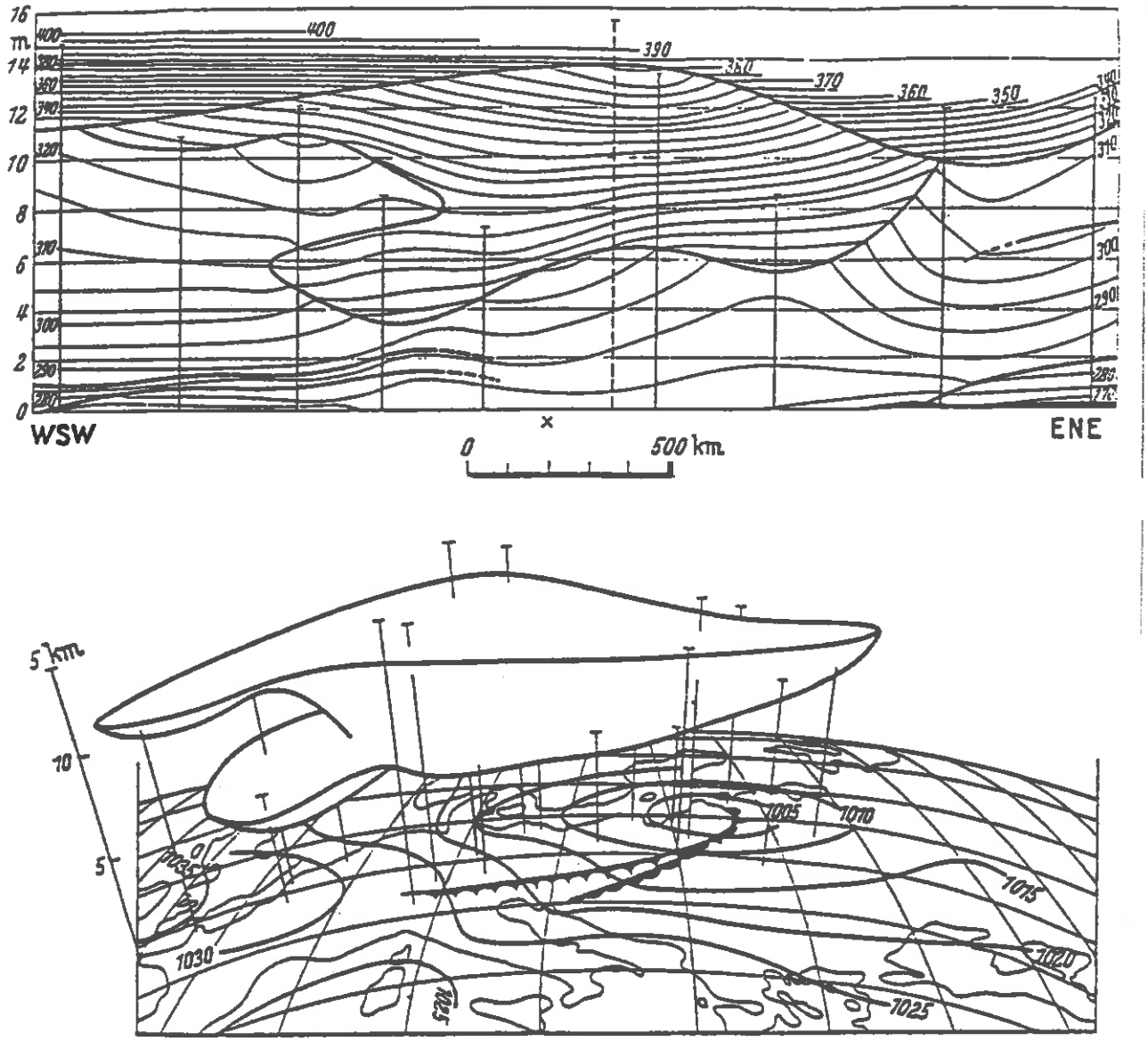

Figure 1: (a) A vertical cross-section through the cyclone of 6 March 1943 at 05Z showing isentropes. Note the outlined body of increased static stability between the troposphere and stratosphere. This elevated body (Höhenkörper) is associated, by Kleinschmidt, with high PV of a value intermediate between that of the lower troposphere and the stratosphere. This figure appeared as figure 2 of (3). (b) A three-dimensional depiction of the Höhenkörper itself above the surface synoptic chart. This appeared as figure 4 of (3).

ESE". He claims that the body then comes over another depression in the western Mediterranean which then begins to develop anew. It is interesting to note that this remark is of some importance since an upper-level PV-streamer stretching southward towards the Alps is now regarded as a significant feature of Alpine lee-cyclogenesis (Bleck and Mattocks (1984) and Volkert et al (1991)). In summary, Kleinschmidt says that ".... the body has nothing to do with the surface depression. It is an independent formation, drifting along with the general high altitude current and ...wherever it arrives it disrupts the existing situation".

This description has similarities to the type-B cyclogenesis events proposed by Petterssen and Smebye (1971). On the basis of numerous synoptic analyses of cyclogenesis these authors classified two types of development. Type-B essentially relies on the progression of an upper level trough to initiate and promote cyclogenesis. Kleinschmidt was not the only scientist to use potential vorticity in synoptic anaysis in the 1950's. Reed (1955) made extensive use of it in discussing upper frontogenesis. Later Danielsen (1968) interpreted tropospheric-stratospheric exchange in terms of potential vorticity and Shapiro (1976 for example) has also discussed observations of the potential vorticity structure of tropopause disturbances.

The next part of that paper (3) presents a theoretical model of the atmosphere including this lentiform body. The important initial step is to identify the region of higher static stability with the more general concept of potential vorticity. This quantity is introduced by reference to Ertel and its properties as an air-mass tracer in the absence of frictional or diabatic processes are noted. The model involves prescribing the PV distribution in a circular region and finding and solving equations for the consistent gradient wind flow and temperature fields. This process has been called the "invertibility principle" by Hoskins et al (1985). Kleinschmidt states that ".....the model.....is less a matter of reproducing reality than of presenting a vivid example which might clearly demonstrate some basic facts". The distribution of PV used is very interesting with a uniform value of 0.3 PVU in the bulk of the troposphere, 2.4 PVU in the stratosphere, and in the lens in the upper troposphere values rising to 1.5 PVU at its centre. (note that 1 PVU $=10^{-6}Km^2s^{-1}kg^{-1}$). This distribution is shown in figure 2 (which reproduces figure 8 of (3)).

There is a peak of PV in the core of the cyclone in the "troposphere" at about 9 km decreasing slightly before stratospheric values are reached at about 13 km. The solution of the inversion equation given on the right-hand-side of the figure for the wind speed and temperature is approximate as he describes various approximations to allow analytical solution in the form of Bessel functions. Numerical solutions of the exact inversion equation are given in Thorpe (1986) for somewhat simpler PV distributions.

The realism of the cyclonic vorticity, surface pressure, and winds of the balanced vortex solution suggests that "A cyclone (or an anticyclone) can only exist if it contains masses with an anomalous Z, i.e. if the function Z (θ) on a vertical line in the interior of the cyclone has other values than those outside". This is elevated to the status of a theorem "... at some altitude within a cyclone there must be masses with excessive values of Z and in an anticyclone there must be masses with a low Z". The paper closes with the only question left namely what is the origin of the anomalous PV? He lists the two possibilities of advection or "..... the cyclone body is newly created during the cyclogenesis .... which can only happen by a non-adiabatic process".

These ideas are interesting from two viewpoints aside from the general importance of the invertibility principle that is postulated. It is clear that even if Kleinschmidt had read Eady or Charney's work he did not appreciate the importance of surface baroclinicity to cyclone development. All the PV inversions done in (3) take zero surface baroclinicity. Following the work of Bretherton (1966) such temperature gradients can be thought of as surrogate anomalous PV. In fact the Eady model, for example, was not originally couched in terms of PV but we now recognize that such baroclinic instability can even occur in an atmosphere with uniform PV but with baroclinicity at the ground and at the tropopause phase-locked (see Hoskins et al. 1985). This is not to say that that is the way cyclones in the atmosphere develop and it is still an open question as to the relative importance in observed cyclones of boundary thermal gradients as opposed to anomalous PV as imagined by Kleinschmidt.

The second aspect of interest is the notion of a body in the upper troposphere of distinct PV with

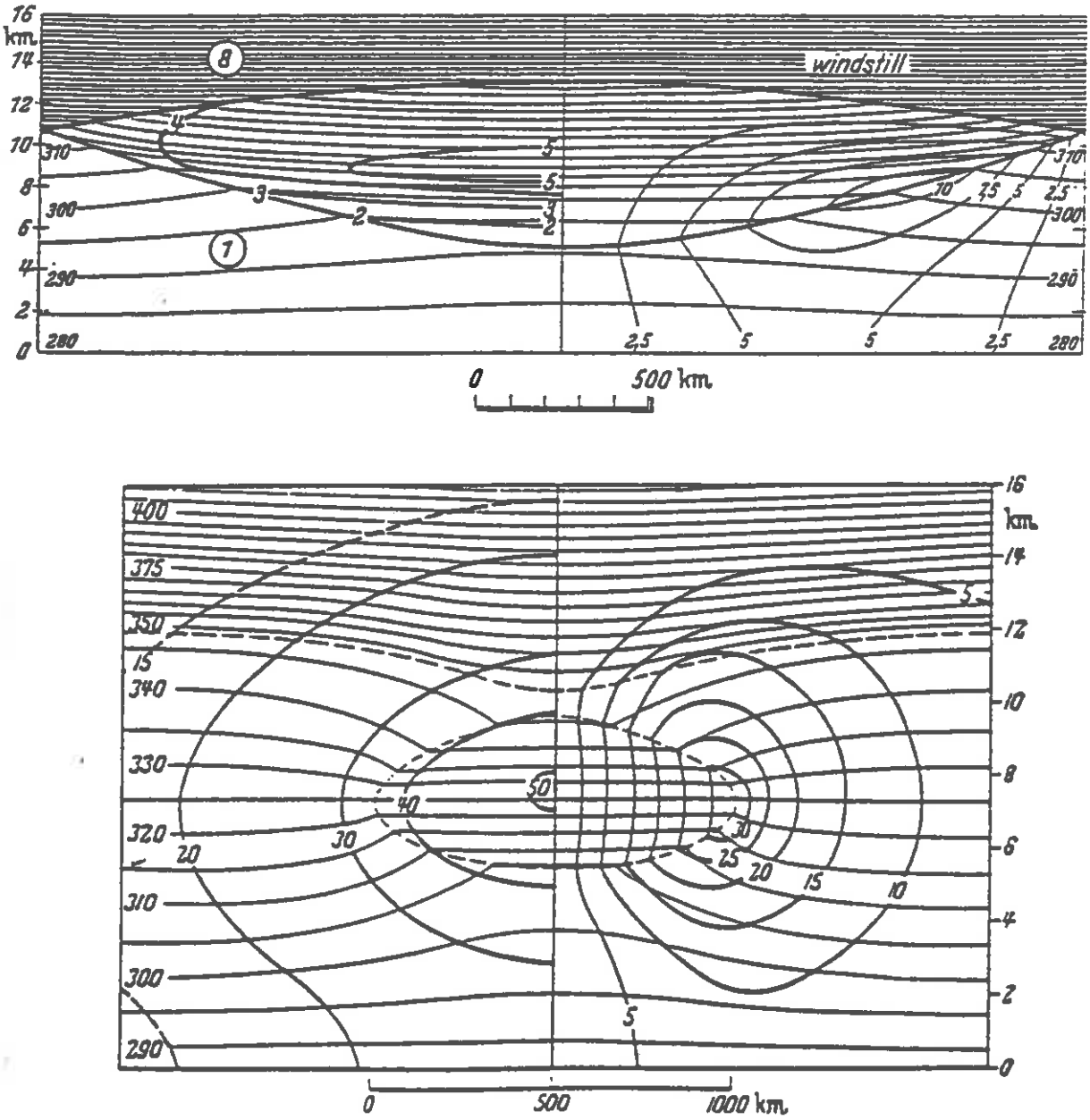

Figure 2: (a) Kleinschmidt's first application of the invertibility principle for a circular vortex satisfying gradient wind and hydrostatic balance. On the left in bold are the assumed contours of potential vorticity varying between 1 unit (0.3 PVU) in the lower troposphere to 8 units (2.4 PVU) in the stratosphere. Note the lentiform body of high PV in the upper troposphere representing the cause of the tropopause cyclone. On the right is the solution of the inversion equation for tangential wind in m/s and for the isentropes. This appeared as figure 8 in (3). (b) The more refined solution as given in figure 23 of (10). Here the lentiform body has uniform PV of 6 times the tropospheric value. On the left are isentropes and relative pressure anomaly in mbar and on the right are isotachs in m/s.

a value intermediate between typical tropospheric and stratospheric values. This does not accord with the general view held now that in fact type-B cyclogenesis is associated with an upper trough or local depression of the tropopause. In the modern view we would probably cast doubt on whether observational errors in analysing PV were such that Kleinschmidt's intermediate values of PV were in fact really stratospheric values. However it is the belief of the author that insufficient high-quality analyses of PV in the troposphere have been made to identify whether intermediate masses, such as those described by Kleinschmidt, exist or not. Perhaps this is still a hypothesis which needs to be assessed as analysis methods improve. It is interesting that in the later summary of these ideas in the review with Eliassen (10) a much clearer mathematical formulation is given and a solution is presented for a lentiform body with uniform PV of 6 times the background tropospheric value but which is still separated from the stratosphere. Despite this separation these cyclones are referred to in (10) as tropopause cyclones and the existence of a distinct tropospheric anomaly is downplayed compared to that which is produced by a deformed tropopause geometry. The idea in (10) that these tropopause cyclones appear "...closely connected with the upper-air flow pattern" even more emphasises the similarity with the type-B cyclogenesis postulated later by Petterson and Smebye (1971).

In the third part of the paper (6) the origin of increased PV at various levels is pursued in another case study of 17 December 1949. The analysis presents calculations of isentropic distributions of PV on the 338, 308, and 288 K surfaces at 12 hr intervals over a 24 hr period. The advective origin of an upper level PV maximum is described. The origin of the structure of the PV field at lower levels is the subject of the second part of the paper (4) on frontal cyclones.

4 Frontal cyclones

In the second part of his set of papers on the origin and structure of cyclones (4) Kleinschmidt pursues the mechanism by which an air-mass can acquire anomalously large PV and thus create a cyclone. (Note that this paper also forms the basis of the description in (10) of frontal cyclones). This is done using another case study of a cyclone or rather the family of cyclones of 16 November 1943 occurring over central Europe. In the introduction he says that "We shall see that it is the condensation process connected with the frontal wave, the so-called upgliding rain (Aufgleitregen) which creates the body of the cyclones". As already described the term "body" refers to an air-mass with anomalous PV. In (10) the word "body" is replaced by "producing mass" in the sense of the mass of high PV which is responsible for producing the cyclone. The synoptic analysis shows a polar front stretching from north-eastern Russia to the central Mediterranean along which 3 frontal cyclones develop. Kleinschmidt concentrates on one of these three developments.

In figure 3 we reproduce figure 3 of (4), which is a vertical cross-section through the warm-front of the cyclone. It is a triumph of draughtsmanship as well as of synoptic analysis.

The theory is in two parts which are not clearly separated from one another. The first is the notion that the growth of the frontal cyclone is due to moist dynamic instability and the second is that PV is increased in the lower troposphere and decreased in the upper troposphere due to latent heat release. Both of these mechanisms are invoked for the development of the cyclone. It seems, but it is difficult to be certain, that Kleinschmidt had in mind a two stage process in which moist symmetric instability is the cause of the earliest growth whereas the PV anomalies are fundamental in maintaining the cyclone.

In figure 3 there is clear evidence of the vorticity vector lying parallel to the θ_e lines which is the neutral condition for moist symmetric instability. Kleinschmidt seems to regard this feature as indicative of actual instability. Considerable emphasis has been placed recently on the neutral condition in frontal zones by Emanuel (1985) and on actual instability by Sanders and Bosart (1985); the issue of whether there is actual moist symmetric instability or merely a tendency to approach neutral conditions from the stable side is still an important and unresolved one. It seems likely that Kleinschmidt uses the existence of the neutral condition in the developed cyclone as a proxy indication of previously existing unstable conditions in the cyclone growth phase. As part of his discussion on symmetric instability Kleinschmidt notes that the criterion for the instability is that the PV must be negative; this was independently deduced later by Hoskins

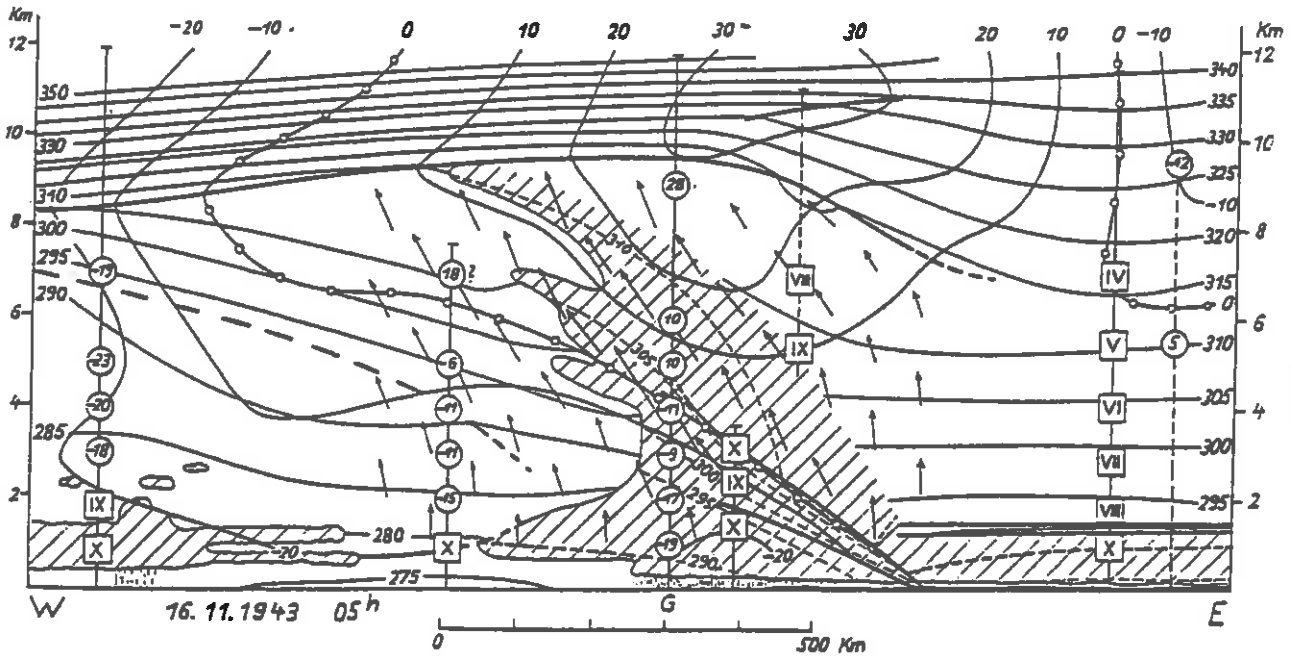

Figure 3: A vertical cross-section through the warm front of the frontal cyclone on 16 November 1943, viewed towards the south. The plotted lines are as follows: thin continuous - θ, thin dashed - θ_w, thick continuous and thick dashed - discontinuous temperature gradients, medium continuous - normal component of the geostrophic wind in m/s, numbers in circles - normal component of the observed wind in m/s, Roman numerals - relative humidity coded as VII = 70-79%, IX = 90-95%, X = over 95%, arrows - absolute geostrophic vorticity vectors, shading - cloud with rainfall shown. The cyclone is moving at 15 m/s towards the north and all winds are relative to the cyclone motion. This appeared as figure 3 in (4).

(1974).

Kleinschmidt then suggests that at a local zone along a quasi two-dimensional front a cloud forms due to moist symmetric instability. Neighbouring regions of the front remain unsaturated thus providing the local spin-up of the nascent cyclone. Of course the theory of conditional symmetric instability relates to a strictly two-dimensional flow and cloud , see Bennetts and Hoskins (1979). The notion of this instability occuring in an essentially three-dimensional form awaits a theoretical justification.

As Kleinschmidt puts it "We now ... tackle the real problem, namely the origin of the cyclone body. To anticipate the solution: in the masses of the lower tropospheric flow Z is greatly increased during its passage through the rain zone". It is interesting to note that in the later review article with Eliassen (10) the emphasis on moist symmetric instability as the causative mechanism is much reduced and the creation of the producing mass of high PV is advanced as the primary mechanism. The analysis proceeds by constructing, on the basis of an assumption of steady flow, 5 trajectories through the cyclone. From this the substantially different three-dimensional flow of air through the cyclone at upper and lower levels is identified. No attempt is made to diagnose the PV itself from the observations; rather its rate of change along trajectories due to latent heat release is calculated. To compute the latent heat release the vertical velocity is estimated from the horizontal winds and the slope of the θ_e lines. Kleinschmidt deduces that the PV should increase by 1.1 PVU on a parcel during its ascent from the surface to a height of 3.3 km along the frontal surface. Hence he proposes that we should expect to see a PV value in the lower troposphere of 2 to 3 times the surrounding value. In the third part of this paper (6) he presents the distribution of potential vorticity on the 288 K isentropic surface for a different synoptic case; indeed there is a ribbon of high values in the warm frontal region at these low levels. That this distribution is commonplace is lent credence from recent analyses of PV using synoptic observations at cold fronts by Hoskins and Berrisford (1988) and by Joly and Thorpe (1990).

In the upper troposphere Kleinschmidt notes that "The increase in Z in the lower flow and the formation of the cyclone body are only one half of the condensation effect.... the upper flow suffers a decrease in Z when it traverses the condensation area..... the reduced Z in the upper flow leads to the building up of an anticyclone in the area ahead of the frontal wave". This description anticipates the later proof that the decrease in Z must exactly equal the increase in Z as a mass-weighted volume integral, Thorpe and Emanuel (1985). The mean vertical shear of the frontal zone is invoked to allow a horizontal separation of the lower cyclone and upper anticyclone. This separation is crucial because if "....cyclonic and anticyclonic masses are above one another they cancel themselves out .....the gradient wind achieves a speed of only a few m/s. It is only when the parts are separated that they achieve their full effect and demand wind fields with considerable energy".

There is little doubt that this description is more akin to type-A cyclogenesis as classified by Petterssen and Smebye (1971). Type-A is the development of a cyclone on a, possibly broad, baroclinic zone without the support of an upper-level disturbance. An attempt to put mathematical substance into Kleinschmidt's model has recently been made by Joly and Thorpe (1990). More detailed synoptic and mesoscale analysis of field observations is needed to clarify which of these mechanisms is the more commonplace.

In a postscript to this work Kleinschmidt returned to the topic in the last paper he published in 1969 (17) with G-M Peter. The theme is much the same and it acts as a useful summary here to quote the abstract of that paper: "According to simple theoretical considerations it is a necessary and sufficient condition for cyclogenesis that, in a completely bounded airmass, the potential vorticity increases. In the particular case studied here one finds that in the central part of the cyclone the potential vorticity increases greatly. Everything indicates that this increase is due to the condensation of water vapor in the region of upgliding motion. For a tropopause funnel developing in connection with the surface cyclone the analysis shows that its origin is at least partly due to diabatic cooling in the middle troposphere".

Nothing is said by Kleinschmidt about the formation of the front itself. In common with the Norwegians he considers the main problem to be to explain the development of the cyclones. The evolution of a distinct warm and cold front in the nascent frontal cyclone is described by

Kleinschmidt as being a consequence of the air-flow curvature consistent with the development of the PV structure. Note that the PV also plays a central role in the semi-geostrophic theory of frontogenesis and cyclogenesis (Hoskins, 1982). There the baroclinic wave develops into a mature cyclone in semi-geostrophic simulations using the constraint of uniform tropospheric PV (Hoskins and West, 1979 and Schär, 1989). Inevitable in such cyclone evolution is the formation of cold and warm fronts. The role of non-uniform PV, generated by condensation, at idealised fronts has been discussed recently by Emanuel et al (1987) in the context of the semi-geostrophic formulation.

5 Final remarks

Meteorological science owes a lot to the endeavours of German scientists and Ernst Kleinschmidt should have a position alongside the best of this school. His promotion of potential vorticity concepts to explain aspects of mid-latitude and tropical cyclones in the 1950's has, 40 years later, been recognised and these are now at the heart of dynamical thinking.

Kleinschmidt's papers

1. 1941 a: Stabilitätstheorie des geostrophischen Windfeldes (Theory of the stability of the geostrophic wind-field). Ann. Hydr., 69, 305-325.
2. 1941 b: Zur Theorie der labilen Anordnung (On the theory of the unstable condition). Met. Zeit., 58, 157
3. 1950 a: Über Aufbau und Entstehung von Zyklonen I (On the structure and formation of cyclones). Meteorol. Rdsch. , 3, Teil 1, 1-6.
4. 1950 b: Über Aufbau und Entstehung von Zyklonen II (On the structure and formation of cyclones). Meteorol. Rdsch. , 3, Teil 2, 54-61.
5. 1950 c: Über den Aufbau atmosphärischer Druckgebilde (On the structure of atmospheric pressure systems). Ber. Dtsch. Wetterd. US-Zone Nr 12, 36-40. (Report of German Weather Service US-Zone 12).
6. 1951 a: Über Aufbau und Entstehung von Zyklonen III (On the structure and formation of cyclones).Meteorol. Rdsch. , 4, Teil 3, 89-96.
7. 1951 b: Grundlagen einer Theorie der tropischen Zyklonen (Principles of a theory of tropical cyclones). Arch. Meteorol. Geophys. Bioklimatol., 4A, 53-72.
8. 1951 c: Untersuchung eines Tropopausentrichters mit Hilfe der Ertelschen Wirbelinvarianten Z (Investigation of a tropopause funnel using Ertel's PV). Annalen der Meteorologie, 4, 131-132
9. 1955 : Die Entstehung einer Höhenzyklone über Nordamerika (The formation of a high-level cyclone over North America). Tellus, 7, 96-108.
10. 1957 : Chapters IV and V in "Dynamic Meteorology" by A. Eliassen and E. Kleinschmidt, Handbuch der Physik, 48, 112-129.
11. 1959 : Nicht-adiabatische Abkühlungen im Bereich des Jetstream (Non-adiabatic cooling in the jetstream regime). Beitr. Phys. Atmosph., 32, 94-108.
12. 1960 : An example of strong diabatic cooling over the Rocky mountains. Dept. of Meteorology, Univ. of Chicago, September.
13. 1965 a: Ageostrophische Windfelder in der hohen Troposphare (Ageostrophic wind-fields in the high troposphere), Beitr. Phys. Atmosph. 38, 28-40.
14. 1965 b: Meteorologische Anwendungen, Abschnitt 8 an "Führer durch die Strömunglehre", 6. und 7. Auflage, (Meteorological Applications, chapter 8 in Guide through fluid mechanics, 6th and 7th editions), by L Prandtl. Braunschweig: Vieweg.
15. 1966 : Über eine Konvektionsströmung (On a convective flow), Beitr. Phys. Atmosph., 39, 235-246.
16. 1967 : Über eine Antizyklone mit starker ageostrophischer Komponente (On an anticyclone with strong ageostrophic components), Offenbach, DWD, Ann. Met.(Neue Folge), 3, 65-71.

17. 1969 : Das Feld der potentiellen Vorticity während einer Zyklonenentwicklung (Potential vorticity field during a cyclonic development) with G-M. Peter , Beitr. Phys. Atm., 42, 67-78.

References

Bennetts D A and Hoskins B J, 1979: Conditional symmetric instability: a possible explanation for frontal rainbands. Q J R Meteorol Soc, 105, 945-962.

Bleck R and Mattocks C, 1984: A preliminary analysis of the role of potential vorticity in Alpine lee cyclogenesis. Contrib. Atmos. Phys., 57, 357-368.

Bretherton F P, 1966: Baroclinic instability and the short wavelength cut-off in terms of potential vorticity. Q J R Meteorol Soc, 92, 335-345.

Charney J G, 1947: The dynamics of long-waves in a baroclinic westerly current. J Meteorol, 4, 135-162.

Danielsen E F, 1968: Stratospheric-tropospheric exchange based on radioactivity, ozone, and potential vorticity. J Atmos Sci, 25, 502-518.

Eady E T, 1949: Long waves and cyclone waves. Tellus, 1, 33-52.

Emanuel K A, 1985: Frontal circulations in the presence of small moist symmetric stability. J Atmos Sci, 42, 1062-1071.

Emanuel K A, Fantini M, and Thorpe A J, 1987: Baroclinic instability in an environment of small stability to slantwise moist convection. Part I: two-dimensional models. J Atmos Sci, 44, 1559-1573.

Helmholtz H, 1888: Über atmosphärische Bewegungen I. Sitzungsberichte Akad. Wissenschaften Berlin, 3, 647-663.

Hoskins B J, 1974: The role of potential vorticity in symmetric stability and instability. Q J R Meteorol Soc., 100, 480-482.

Hoskins B J and West N V, 1979: Baroclinic waves and frontogenesis, Part II: uniform potential vorticity jet flows - cold and warm fronts. J Atmos Sci, 36, 1663-1680.

Hoskins B J, 1982: The mathematical theory of frontogenesis. Ann Rev Fluid Mech, 14, 131-151.

Hoskins B J,McIntyre, and Robertson A W, 1985: On the use and significance of isentropic potential vorticity maps, Q J R Meteorol Soc, 111, 877-946.

Hoskins B J and Berrisford P, 1988: The storm of 15/16 October 1987. A potential vorticity perspective, Weather, 43, 122-129.

Joly A and Thorpe A J, 1990: Frontal instability generated by tropospheric potential vorticity anomalies, Q J R Meteorol Soc, 116, 525-560.

Palmén E and Newton, 1969: Atmospheric circulation systems. Academic Press.

Pettersen S and Smebye S J, 1971: On the development of extratropical cyclones, Q J R Meteorol Soc, 97, 457-482.

Reed R J, 1955: A study of a characteristic type of upper-level frontogenesis. J Meteorol, 12, 542-552.

Sanders F and Bosart L F, 1985: Mesoscale structure in the megalopolitan snowstorm of 11-12 February 1983, Part I: Frontogenetical forcing and symmetric instability. J Atmos Sci, 42, 1050-1061.

Schär C J, 1989: Dynamische Aspekte der aussertropischen Zyklogenese, PhD thesis, ETH, Zürich, pp 241.

Shapiro M A, 1976: The role of turbulent heat flux in the generation of potential vorticity in the vicinity of upper-level jet stream systems. Mon Wea Rev, 104, 892-900.

Solberg H, 1928: Integrationen der atmosphärischen Störungsgleichungen, Geophys. Publ., 5, 9.

Thorpe A J, 1986: Synoptic scale disturbances with circular symmetry. Mon Wea Rev, 114, 1384-1389.

Thorpe A J, 1993: An appreciation of the meteorological research of Ernst Kleinschmidt. Meteorol. Zeitschrift, N.F. 2, 3-12.

Thorpe A J and Emanuel K A, 1985: Frontogenesis in the presence of small stability to slantwise convection J Atmos Sci, 42, 1809-1824.

Volkert H, Weickmann L, and Tafferner A, 1991: The Papal front of 3 May 1987: a remarkable example of frontogenesis near the Alps. Q J R Meteorol Soc, 117, 125-150.

AIRFLOW AND STRUCTURE OF PRECIPITATION SYSTEMS IN EXTRATROPICAL CYCLONES

K A Browning

Joint Centre for Mesoscale Meteorology*
University of Reading, UK

1. INTRODUCTION

A review of this topic (Browning 1990) was presented at the Palmén Memorial Symposium on Extratropical Cyclones held in Helsinki in 1988. That review covered a wide range of precipitation systems but it concentrated mainly upon systems associated with fronts away from areas of major development. In recent years the focus of research activity has shifted towards rapidly developing cyclones. Much research has been oriented towards the dynamics but there have also been some advances in our understanding of how the precipitation in such systems relates to the dynamical structure. The purpose of this review, six years after the Palmén Symposium, is to extend the ideas about precipitation systems that I presented then to a set of situations accompanying cyclone development. A feature common to the situations to be considered is the presence of an upper-level maximum of potential vorticity (PV) overrunning a low-level baroclinic zone, itself characterized by high PV, generated diabatically.

This review has two components. In Section 2 a conceptual framework is outlined which contains components that are adapted in later sections to the particular circumstances associated with an overrunning upper-level PV maximum. The framework in Section 2 is taken directly from Browning (1990). It is based upon the simple concept of different configurations of major airflows producing particular kinds of frontal archetype. The major airflows, referred to as conveyor belts and dry intrusions, are visualized as system-relative isentropic flows that relate well to the patterns of precipitation and cloud seen in radar and satellite imagery.

2. FRAMEWORK FOR DIAGNOSING FRONTAL PRECIPITATION STRUCTURE

Airstreams called conveyor belts are a convenient way of visualizing the overall organization. The Warm Conveyor Belt (WCB) is a stream of air with high wet-bulb potential temperature (θ_w) travelling rapidly along a cold front. Often the WCB is characterized by a neutrally stratified low-level jet just ahead of the front. Although the main component of motion within the WCB is parallel to the cold front, the ageostrophic components of motion perpendicular to the front can be quite large and have an important bearing on the frontal structure. It is useful to distinguish two situations that lead to contrasting organizations of cloud and precipitation:

2.1 Rearward-sloping ascent

The "rearward-sloping ascent" archetype is one in which the air in the WCB has a component of motion rearward relative to the movement of the cold front and in which the main slantwise ascent occurs above the cold frontal zone (Fig 1). This is the classical cold frontal archetype, known as an ana-cold front, in which the warm air rising slantwise over the cold air leads to a Wide Cold Frontal Rainband (WCFR) (Fig 2) (Houze et al 1976); sometimes the WCFR is broken up into multiple WCFRs probably due to conditional symmetric instability (Bennetts and Hoskins 1979). The cold frontal zone penetrates to the ground as a sharp surface cold front where the cold air sometimes appears to behave as a density current, forcing the air in the WCB to rise abruptly through 2 or 3 km in the form of line convection (Fig 1) and producing a Narrow Cold Frontal Rainband (NCFR) that is usually segmented as in Fig 2.

* The Joint Centre for Mesoscale Meteorology is supported by the Meteorological Office and the Department of Meteorology, University of Reading.

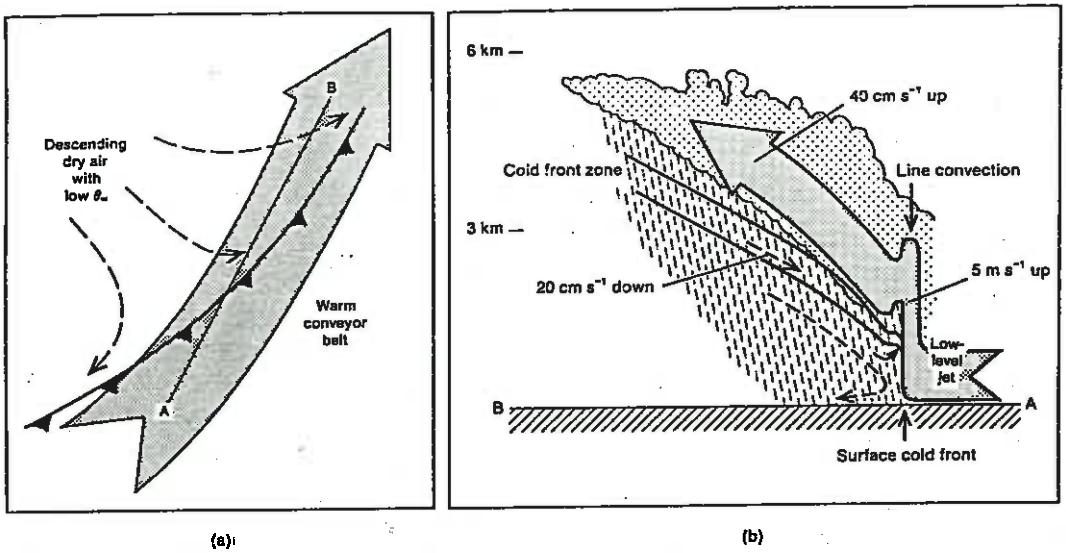

Figure 1. Schematic portrayal of the airflow at a classical ana-cold front showing the warm conveyor belt (bold arrow) undergoing rearward-sloping ascent above the cold frontal zone, with the cold air (dashed lines) descending beneath it: (a) plan view; (b) vertical section along AB in (a). Flows are shown relative to the moving frontal system.

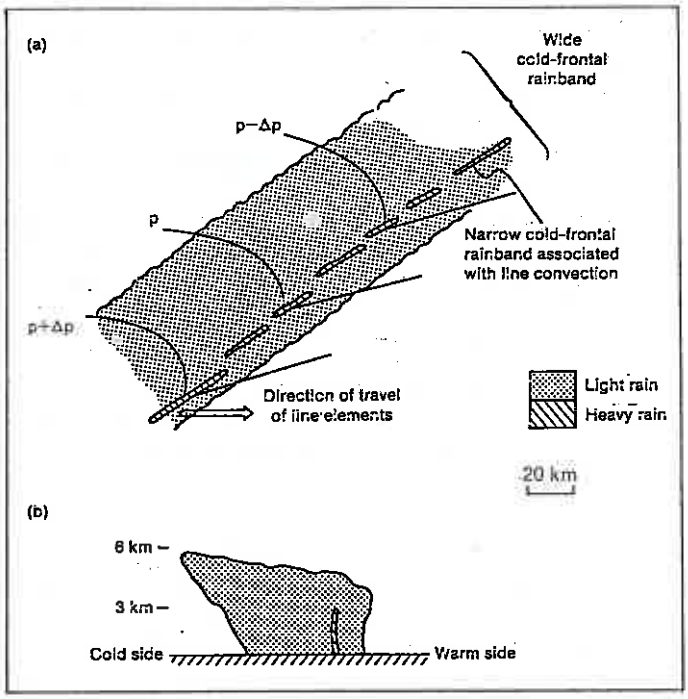

Figure 2. Schematic depiction of the precipitation distribution at a sharp ana-cold front (a) in plan view and (b) in a vertical cross section normal to the front.

2.2 Forward-sloping ascent

The second archetypal situation is the "forward-sloping ascent" configuration of the WCB, in which the air in and above the WCB has a component of motion forward relative to the movement of the cold front (Fig 3), with its main region of slantwise ascent occurring farther downwind at a classical ana-warm front. The cold front in this case is referred to as a kata-cold front.

Figure 3. Schematic portrayal of the airflow in an extratropical cyclone in which the warm conveyor belt (stippled arrow) is undergoing forward-sloping ascent ahead of a kata-cold front, before rising above a flow of cold air ahead of the warm front (dotted arrow referred to as the cold conveyor belt). Dry middle-tropospheric air with low θ_w is shown overrunning the cold front and generating potential instability at the top of the warm conveyor belt. Plan view and vertical section are shown in (a) and (b), respectively, the section in (b) being along the line AB in (a). Flows are shown relative to the moving frontal system.

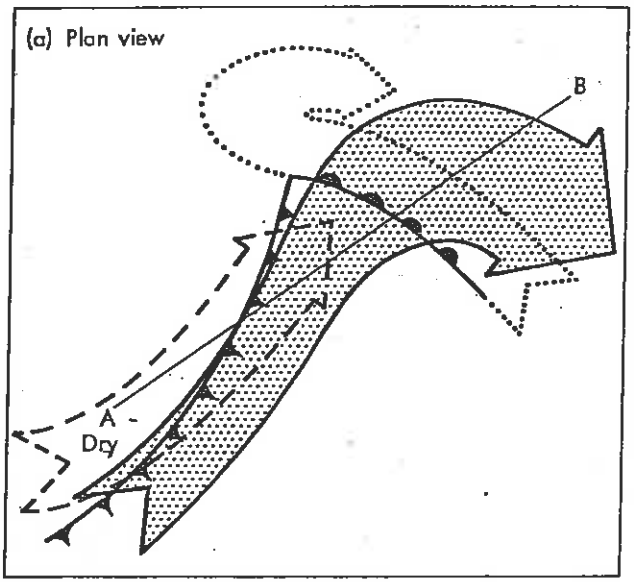

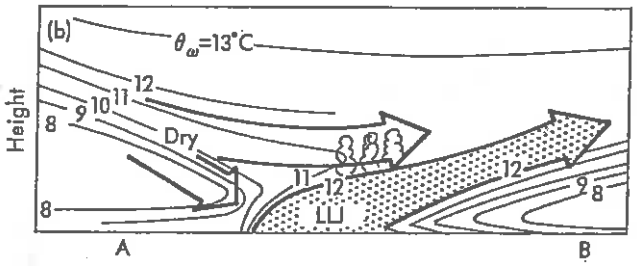

A characteristic feature of this archetype is the dry low-θ_w air that overruns the surface cold front (SCF) and advances some distance ahead of it, confining the high-θ_w air of the WCB within a shallow moist zone (SMZ) only 2 or 3 km deep. This dry airstream is called the dry intrusion. Although ascending by the time it overruns the WCB, the dry intrusion has had a previous history of descent from the upper troposphere and sometimes from the lower stratosphere - hence it is sometimes referred to as a stratospheric intrusion. The dry (or stratospheric) intrusion is one of the symptoms of an approaching upper-level PV maximum and it may be revealed in satellite water vapour imagery as a so-called dark zone or dry slot.

The dry intrusion has a profound effect on the structure of the precipitation. The low-θ_w air in the dry intrusion has a high dry-bulb potential temperature (θ) where it begins to overrun the high-θ_w air in the WCB but large-scale ascent eventually realises the potential instability. This often happens at the leading edge of the dry intrusion which fills up with air convecting from the WCB and this becomes the upper cold front (UCF). The existence of horizontally separated SCF and UCF gives rise to the name 'split front' (Browning and Monk 1982). The SCF and UCF are usually well-defined as moisture fronts and as θ_w-fronts but sometimes are not well defined as temperature fronts.

There are three main regions of precipitation associated with the forward-sloping ascent archetype (Fig 4):

- Warm frontal precipitation. This is usually in the form of a wide frontal rainband associated with broad-scale slantwise ascent, although, as in the case of the cold frontal rainbands, conditional symmetric instability may lead to multiple mesoscale bandedness parallel to the frontal zone. Beneath the warm frontal zone low-θ_w air flows towards the cyclone centre as shown by the dotted arrows in Fig 3(a). This is the cold conveyor belt (CCB) (Carlson 1980). It can be a strong flow relative to the system, especially where it approaches the cyclone centre. It begins as a dry airstream originating from subsided air from the dry intrusion left behind by a previous cyclone system, and much of the warm frontal precipitation falling below the warm frontal zone evaporates into it. At first the CCB air descends, this being enhanced locally by evaporative cooling. As the CCB approaches the cyclone centre it begins to ascend and this leads to the characteristic patterns of cloud and precipitation discussed in Sec 3.

- Precipitation associated with the upper cold front. A band of heavier precipitation often occurs at the leading edge of the dry intrusion. This is due to mid-tropospheric convection of high-θ_w air from the WCB into the overrunning low-θ_w air, as discussed above. Often these convective cells occur above a region of saturated slantwise ascent and the precipitation particles continue to grow as they fall beneath the convective cells.

- Outbreaks of convective rain within the shallow moist zone (SMZ) between the SCF and UCF. Shallow boundary layer convection often breaks out, and leads to patches of light rain and drizzle, within the SMZ. At the SCF itself the convergence may be sufficient to produce a more organized band of shallow precipitation. Sometimes, in a rapidly deepening cyclone, a band of deep convection breaks out between the SCF and UCF, perhaps leading to a major squall line.

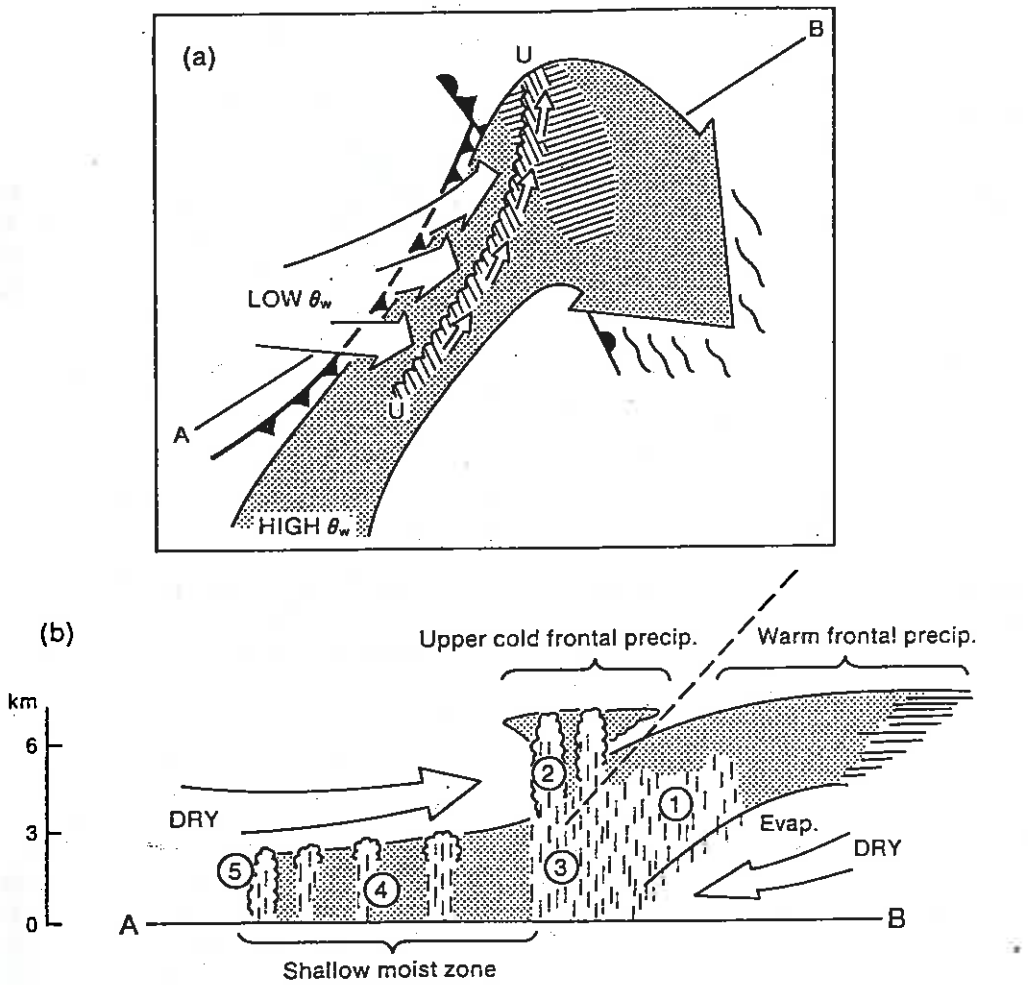

Figure 4. Schematic portrayal of the same archetype as in Fig 3 with the warm conveyor belt undergoing forward-sloping ascent, but drawing attention to the split-front characteristics and the overall distribution of precipitation: (a) plan view; (b) vertical section along AB in (a). In (a) UU represents the upper cold front or moisture front. The hatched shading along UU and ahead of the warm front represents precipitation associated with the upper cold front and warm front, respectively. Numbers in (b) represent precipitation types as follows: (1) warm frontal precipitation; (2) convective precipitation-generating cells associated with the upper cold front; (3) precipitation from the upper cold frontal convection descending through an area of warm advection; (4) shallow moist zone (SMZ) between the upper and surface cold fronts, characterized by warm advection and scattered outbreaks of mainly light rain and drizzle; and (5) shallow precipitation at the surface cold front itself (Browning and Monk 1982).

3. CLOUD AND PRECIPITATION STRUCTURES ASSOCIATED WITH DEVELOPING CYCLONES

The archetypes described in the previous section apply most straightforwardly to places away from regions of cyclogenesis: Figs 1 and 2 relate to the trailing part of a cold front and Figs 3 and 4 relate to parts of a cyclonic system south of its centre prior to any period of significant development. As soon as significant cyclogenesis occurs both the airflow configuration near the cyclone centre, and the associated cloud and precipitation, take on a characteristic structure which is the subject of this section. Amongst the changes that occur is a strengthening of the CCB flow. Initially most of this flow turns anticyclonically in the manner shown by the dotted arrow in Fig 3(a). When the cyclone begins to deepen some of the CCB air turns cyclonically as part of a strongly diffluent flow. The diffluent flow at the head of the CCB gives rise to one of the most obvious features of the developing cyclone, the cloud head, to be described shortly.

The structure we shall be describing can be related to Shapiro and Keysers' (1990) life-cycle model of a frontal cyclone (Fig 5). This represents a process, referred to as frontal fracture, in which the fractured cold front moves along the warm front away from the cyclone centre, leaving behind a 'bent back warm front' that eventually wraps around the cyclone centre. We shall focus, in this section, on the structure during their Stage II.

The cold and warm air currents (arrows) sketched in Fig 5(b) correspond to portions of the CCB and WCB where these are close to the surface. The WCB, beyond the tip of the dashed arrow in Fig 5(b), goes on to ascend above the warm front. A closer look at the CCB shows that it actually fans out, as previously mentioned, with some of it following the solid arrow cyclonically in Fig 5(b) and some ascending anticyclonically as in the dotted arrow in Fig 3. A representation of this flow pattern and the associated cloud and precipitation is shown in Fig 6. It is shown in four parts to minimize confusion but the reader will need to imagine them combined into one diagram in order to visualize the interrelationships.

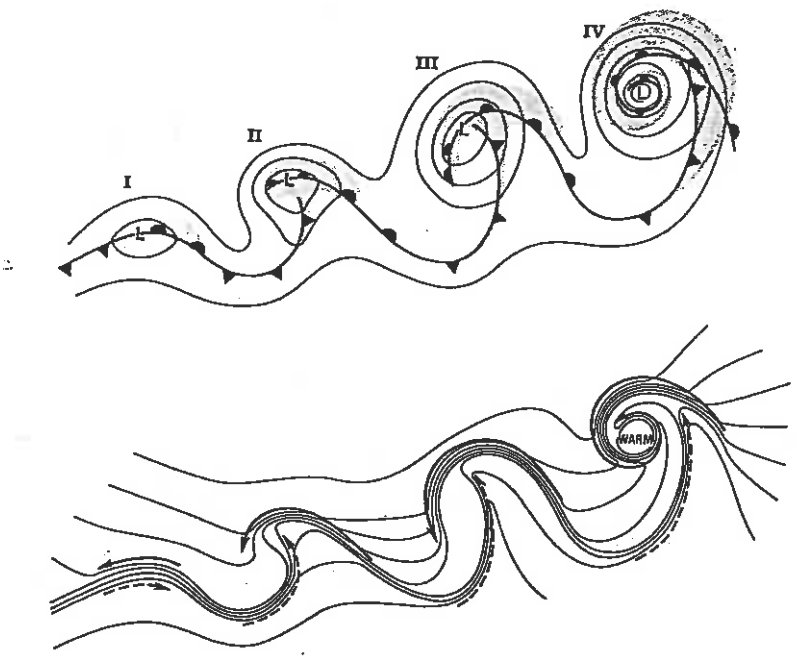

Figure 5. The life cycle of a marine extratropical frontal cyclone (Shapiro and Keyser 1990): (I) incipient frontal cyclone; (II) frontal fracture; (III) bent-back warm front and frontal T-bone; (IV) warm-core frontal seclusion. Upper: sea-level pressure, solid lines; fronts, bold lines; and cloud signature, shaded. Lower: temperature, solid lines; cold and warm air currents, solid and dashed arrows, respectively.

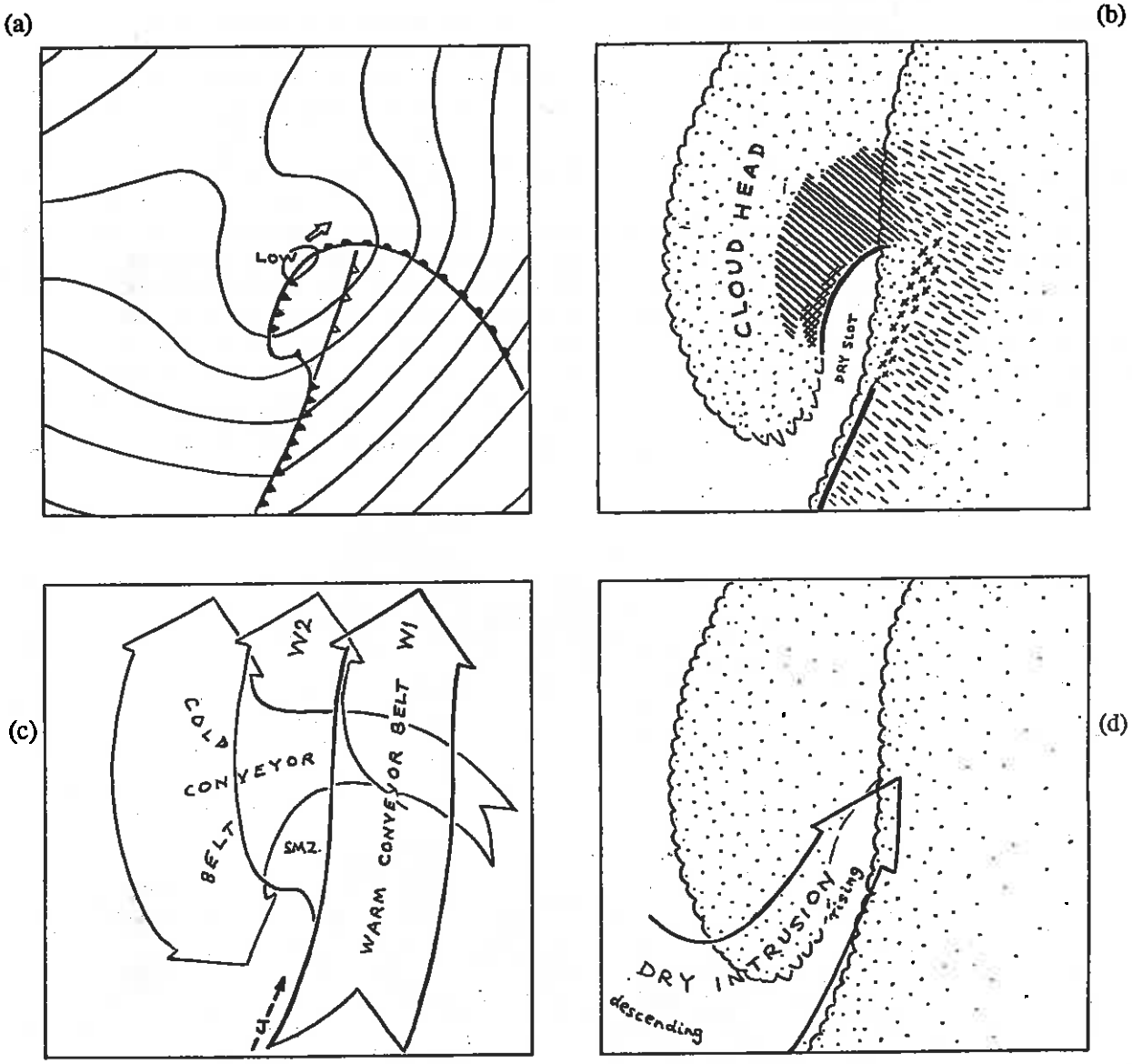
(a)
Low
(b)
CLOUD HEAD
DRY SLOT
(c)
W2
W1
COLD CONVEYOR BELT
SMZ.
WARM CONVEYOR BELT
(d)
DRY INTRUSION
rising
descending

Fig 6

Figure 6 Caption

Airflow and precipitation within a developing extratropical frontal cyclone (based on Browning and Roberts 1994).

(a) Sea-level pressure (4mb intervals) and frontal analysis. The low is travelling towards the NE (top right). Surface warm front is shown conventionally. Part of the so-called bent back warm front is shown as a cold front. The main cold front is shown with closely spaced frontal symbols where it is sharp. The unshaded cold frontal symbols show where it is detectable only aloft (UCF). In between the two sharp surface cold fronts there is a diffuse surface cold front shown by an s-shaped front with a single frontal symbol.

(b) Cloud and surface precipitation analysis. Regions of cloud without surface precipitation are shown stippled. The western boundaries of two major cloud features are drawn scalloped: the cloud feature occupying the left half of the diagram is the cloud head; the cloud occupying the right half is the main polar front cloud band associated with the warm conveyor belt (see W1 in (c)). Precipitation features are depicted as follows:

solid hatching	—	cloud head precipitation, cross-hatched where convective (moderate to heavy)
broken hatching	—	warm conveyor belt precipitation (mainly light intensity)
broken cross-hatching	—	mid-level convective precipitation associated with upper cold front (patchy moderate rain)
solid shading	—	narrow cold frontal rainbands (heavy rain associated with intense shallow line convection)

(c) Conveyor belt analysis. System-relative motion for the three key moist flows:

- Main warm conveyor belt (WCB) labelled W1.
- Lower part of WCB which peels off and ascends as flow W2 in the top part of the cloud head.
- Cold conveyor belt (CCB) whose ascending diffluent flow is responsible for a large proportion of the cloud head and associated precipitation.

The westward component of flow within W1 and the CCB is associated with the ageostrophic transverse circulation at the exit of an upper level jet (position of jet core shown by J).

(d) Dry intrusion analysis. System-relative motion for the dry air that descends from near the tropopause upwind and reascends while approaching the cyclone centre where it overruns a shallow moist zone associated with W2 (see SMZ in (c)).

Key interrelationships in Fig 6 are as follows (letters in brackets refer to parts (a), (b), (c) and (d) of Fig 6):

- The ascending WCB (W1 in c) is responsible for the belt of polar front cloud and light rain shown in Fig 6(b) that lies ahead of the main cold and warm fronts shown in (a).

- The diffluent CCB (c) is bounded by the warm front and the bent back front (a). Its ascent generates the cloud head and associated precipitation; some of this evaporates before reaching the ground and some, closer to the surface front, reaches the surface (b).

- The precipitation within the cloud head is augmented by the ascent of flow W2 (c) which peels off to the left from the lower part of W1. Like the westward-directed flow in the CCB, W1 is associated with a transverse ageostrophic circulation at the exit of an upper tropospheric jet streak accompanying an upper PV maximum. The flow W2 rises over the CCB and constitutes part of the cloud head (b).

- The dry intrusion flow gives rise to the characteristic 'dry slot' between the cloud head and the frontal cloud band (d). Within the dry slot it overruns a shallow moist zone (cf SMZ in Sec 2) associated with W2 where it emerges to the left of W1 (c). The dry intrusion air has a lower θ_w than the W2 flow. The resulting potential instability gives rise to convective precipitation where the lifting is sufficient. Thus the precipitation is usually convective within the part of the cloud head (b) near the left edge of the dry intrusion (d), and also along the upper cold front (a, b) near the leading edge of the dry intrusion (d). Given sufficient large-scale ascent, outbreaks of convective precipitation can occur within the dry slot too.

- The two segments of sharp surface cold front (a) are characterized by narrow cold frontal rainbands (b). These are due to narrow lines of shallow but intense convection as described in Sec 2. Typically this convection may be little more than 3 km wide and 3 km deep.

Often in a rapidly developing cyclone, the main area of precipitation is associated with the area of slantwise ascent within the cloud head rather than within the WCB. In contrast to the precipitation generated within a WCB, where it ascends as part of a thermally direct circulation above a trailing ana-cold front (Fig 1) or above an ana-warm front (Fig 3), a large proportion of the precipitation within a cloud head is due to ascent of CCB air as part of a thermally indirect circulation.

4. GENERALIZED PATTERN OF FLOW ASSOCIATED WITH AN UPPER-LEVEL PV MAXIMUM

Key aspects of the organization in Fig 6 can be conceptualized simply in terms of an interlocking dual flow pattern, as portrayed in Fig 7 and explained in the caption. Essentially, one of the flows consists of dry, low-θ_w air descending from near the tropopause (the dry intrusion) and the other consists of moist air, with a range of θ_w (CCB plus W2), rising from low levels into the cloud head. The flows are a manifestation of an upper-level potential vorticity maximum. Some of the precipitation features discussed above occur in the region where part of the recently descended 'dry intrusion' flow enters the region of ascent and overruns part of the main 'cloud head' flow which itself is characterized by high potential vorticity of diabatic origin.

The splayed-out nature of the two hammer-head flows depicted in Fig 7 is due to the effect of the large-scale deformation field in straining the flow along an axis SSW to NNE. A more nearly symmetrical vortex-like flow pattern, accompanied by a more strongly hook-shaped region of precipitation develops when the deformation field weakens especially if rapid cyclogenesis takes place.

The flow configuration in Fig 7 often occurs close to the main polar front zone and associated WCB, as in Fig 6. However, it also frequently occurs elsewhere. In particular, when the upper PV maximum responsible for it occurs in the cold air a long way from the polar front, a comma cloud pattern somewhat resembling a cloud head develops in which the main WCB flow, W1, plays no part. The comma cloud is characterized by a CCB flow and a flow of relatively warm air, the equivalent of W2 in Fig 6, but it does not draw upon the really warm air from beneath the main WCB flow, W1.

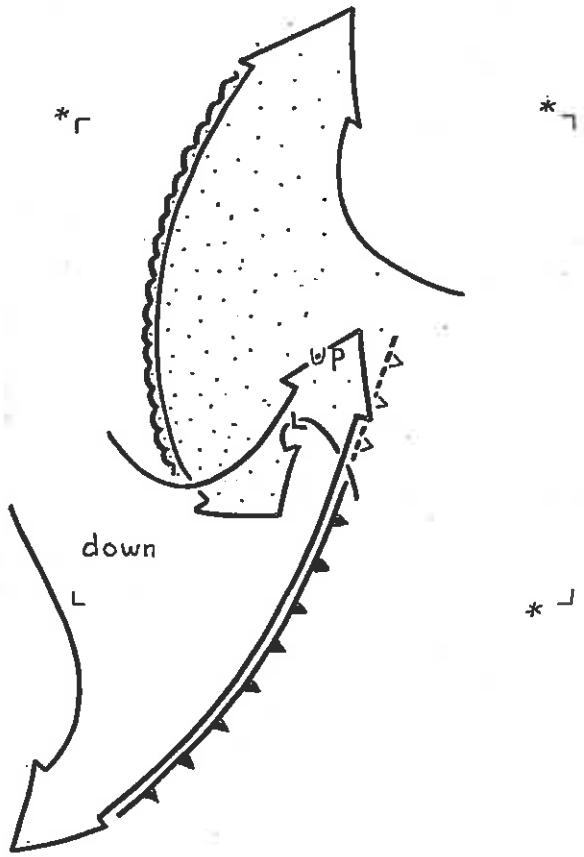

Figure 7. A broader-scale view of the flows responsible for the structures in Fig 6 (neglecting the flow W1). The area of Fig 6 is shown by the four corners denoted by asterisks. Two interleaving and broadly symmetrical flows are shown; each produces a highly diffluent zone at its leading edge. One of them is the dry intrusion that descends from near the tropopause and splays out at low levels behind the cold front. The other is a combination of the two flows identified in Fig 6 as CCB and W2, and as such correspond to air that originates at low levels ahead of and behind the warm front and which subsequently ascends and splays out at high levels within the cloud head, the outer boundary of which is shown scalloped. Part of the dry intrusion overruns the moist cloud head flow in the region of strong upward motion, labelled 'Up'. The cyclone centre is located at L.

Often a polar air vortex that forms separately from the polar front will, as recognized by Zillman and Price (1972), subsequently interact with the main WCB. In such a situation the CCB and W2 flows do still exist as in Fig 6, but they emerge from beneath a polar front cloud band and associated W1 flow that are much farther away from the cyclone centre than in Fig 6. The resulting configuration is referred to as an instant occlusion.

5. THE EFFECT OF MULTIPLE DRY INTRUSIONS IN A DEVELOPING CYCLONE

Sometimes an extratropical cyclone develops in association with a sequence of upper-level PV maxima, each with its own dry intrusion and each influencing the structure of the overall cloud and precipitation system. The separate dry intrusions may be tracked in the satellite water vapour imagery. And each dry intrusion may generate its own cold front. Each dry intrusion may also exhibit further fine structure where its dry air penetrates towards the surface, thereby producing a more complicated pattern of cloud and precipitation.

A case that we have recently analyzed in some detail as part of the FRONTS-92 dropsonde experiment provided an example of a developing cyclone affected by two major dry intrusions having somewhat different propagation velocities. The first of these dry intrusions, along with its cold front, propagated faster than the overall cyclone system. As a result the first cold front, which had been the primary surface feature when the cyclone first began to deepen, overrode the WCB and evolved from a surface front into an upper cold front within a period of hours (Fig 8). The cloud along this cold front was initially too shallow for precipitation, the region being dominated by the descent of the dry intrusion. When the front began to override the WCB, a line of mid-level convective cells broke out. While this was happening the cold front associated with the second dry intrusion took over as the main surface cold front at the poleward boundary of the WCB. The result was a split cold front structure as in Fig 6. Presumably such a structure can evolve either in this discrete manner or more simply by part of a continuous flow of cold air running ahead of the surface cold front.

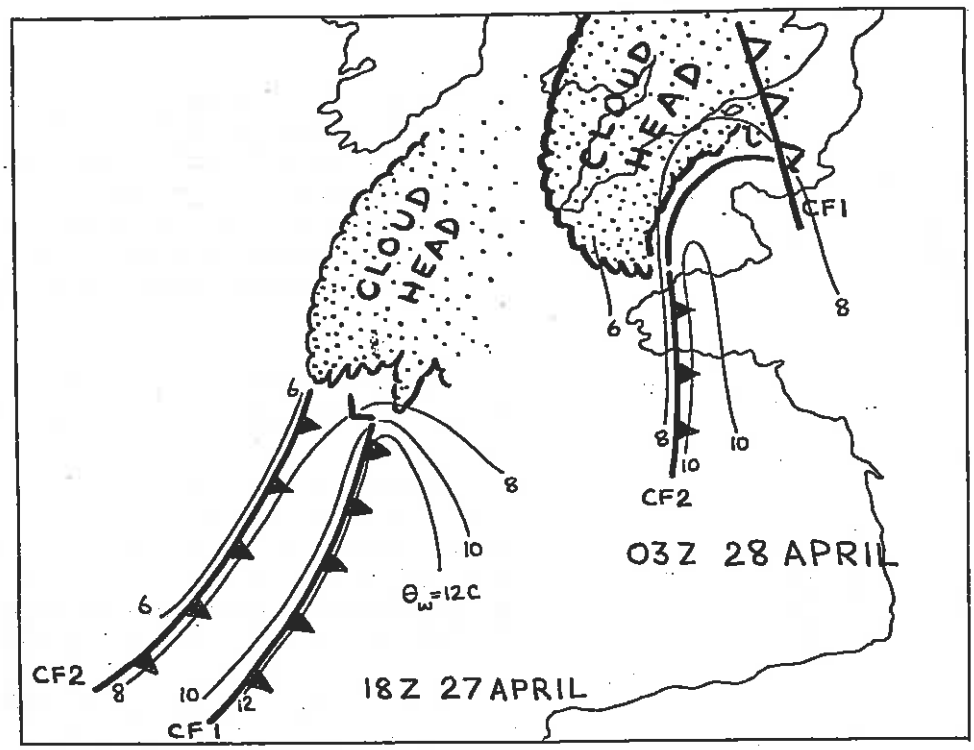

Figure 8. Analysis from FRONTS-92 showing two cold fronts in relation to the cloud head at two times during the rapid deepening of a small frontal cyclone. Thin lines are near-surface θ_w at 2C intervals. The thick line is radar-detected line convection. Notice that the leading cold front evolves from a surface feature (solid cold front symbols) to an upper cold front (open cold front symbols).

6. REFERENCES

Bennetts, D.A., and B.J. Hoskins, 1979: Conditional symmetric instability - a possible explanation for frontal rainbands. *Quart.J.Roy.Meteor.Soc.*, **105**, 945-962.

Browning, K.A., 1990: Organization of clouds and precipitation in extratropical cyclones. In *Extratropical cyclones: the Erik Palmén Memorial Volume*, C.W. Newton and E.O. Holopainen, Eds., American Meteorological Society, 129-153.

Browning, K.A., and G.A. Monk, 1982: A simple model for the synoptic analysis of cold fronts. *Quart.J.Roy.Meteor.Soc.*, **108**, 435-452.

Browning, K.A., and N. Roberts, 1994: Structure of a frontal cyclone. *Quart.J.Roy.Meteor.Soc.*, **120**, In press.

Carlson, T.N., 1980: Airflow through midlatitude cyclones and the comma cloud pattern. *Mon.Wea.Rev.*, **108**, 1498-1509.

Houze, R.A., P.V. Hobbs, K.R. Biswas and W.M. Davies, 1976: Mesoscale rainbands in extratropical cyclones. *Mon.Wea.Rev.*, **104**, 868-878.

Shapiro, M.A., and D. Keyser, 1990: Fronts, jet streams and the tropopause. In *Extratropical cyclones: the Erik Palmén Memorial Volume*, C.W. Newton and E.O. Holopainen, Eds., American Meteorological Society, 167-191.

Zillman, J.W., and P.G. Price, 1972: On the thermal structure of mature Southern Ocean cyclones, *Austral.Meteor.Mag.*, **20**, 34-48.

DEVELOPMENT OF AN ATLANTIC FRONTAL WAVE DURING IOP 3 OF FRONTS 92

Sid A Clough and Clare S A Davitt

Joint Centre for Mesoscale Meteorology,
UK Meteorological Office / University of Reading, UK.

1. INTRODUCTION

The Fronts 92 experiment was set up to study the development of minor and major waves on fronts, an important forecasting problem in the Eastern Atlantic. The case observed during IOP 3 was in fact well forecast 30 hours before the event, and diagnostic studies of the forecast evolution centred on the notion of attributing "sources" to some aspects of the development, for example upper and lower level forcing of vertical motion.

Some recent work (Bishop and Thorpe (1994)) has suggested the value of applying the methods of classical electrostatic theory (point sources and their associated fields) to the use of potential vorticity and the inversion problem. Since the quasigeostrophic omega equation, with proper coordinate scaling, is also readily transformed into Poisson's equation in 3 dimensions the approach can also be applied to the study of sources of vertical motion.

The forcing of vertical motion by the geostrophic flow can be expressed by means of the divergence of the Q vector (hereafter referred to as div Q, see Hoskins, Draghici and Davies (1978)). In many studies the use of div Q has been advocated in forecasting as a surrogate for the vertical velocity pattern, as it does not require solution of a 3-dimensional differential equation. However, as illustrated below, the patterns of div Q found in practice are 3-dimensional and complex, and show a range of scales so that the local patterns of div Q often do not closely correspond to the pattern of the vertical motion. Since there are now readily available library subprograms for the solution of equations like the omega equation, there is actually no need to use div Q itself in many circumstances.

In the course of this work another important point also arose. Since div Q represents the total geostrophic forcing of vertical motion the full 3-dimensional field of div Q, properly interpreted, might be (and in fact is) richer in dynamical information than the simplistic use commonly suggested. Two objectives were seen to be important in the study:

1) To validate quantitatively the use of quasigeostrophic theory through div Q in the practical environment.

2) To understand how the contributions to patterns of div Q in three dimensions are related to the resulting vertical motion.

2. PATTERNS OF DIV Q

Fig 1 illustrates the synoptic pattern at 18UT on 27th April 1992, showing two frontal waves over the Atlantic; the system approaching the UK was observed by C-130 dropsondes in a flight centred upon this time (Hewson (1993)). The pattern of divergence of Q vectors at four levels for the area is illustrated in Fig 2. Note that equal contour intervals are used at all levels. Two main features are evident:

(a) because of the larger wind speeds and temperature gradients near the tropopause the forcing of vertical motion at upper levels greatly exceeds that through most of the troposphere, except near 900 hPa very close to the surface low. At 300 hPa it is about 5 times greater than at 700 hPa.

(b) a pattern of multiple bands is present at all levels, and is most intense at upper levels, where deformation and shear act upon temperature gradients associated with a tongue of warm upper tropospheric air drawn downstream from North America in the previous day.

Because of such complexity the actual pattern of vertical motion is not readily deduced from div Q itself in observations as opposed to idealised models. This is particularly so at 700 hPa, a level commonly used for application of the Q vector because it tends to be the steering level for baroclinic disturbances. Since the forcing of vertical motion due to div Q is actually greatest near the surface and at the tropopause the

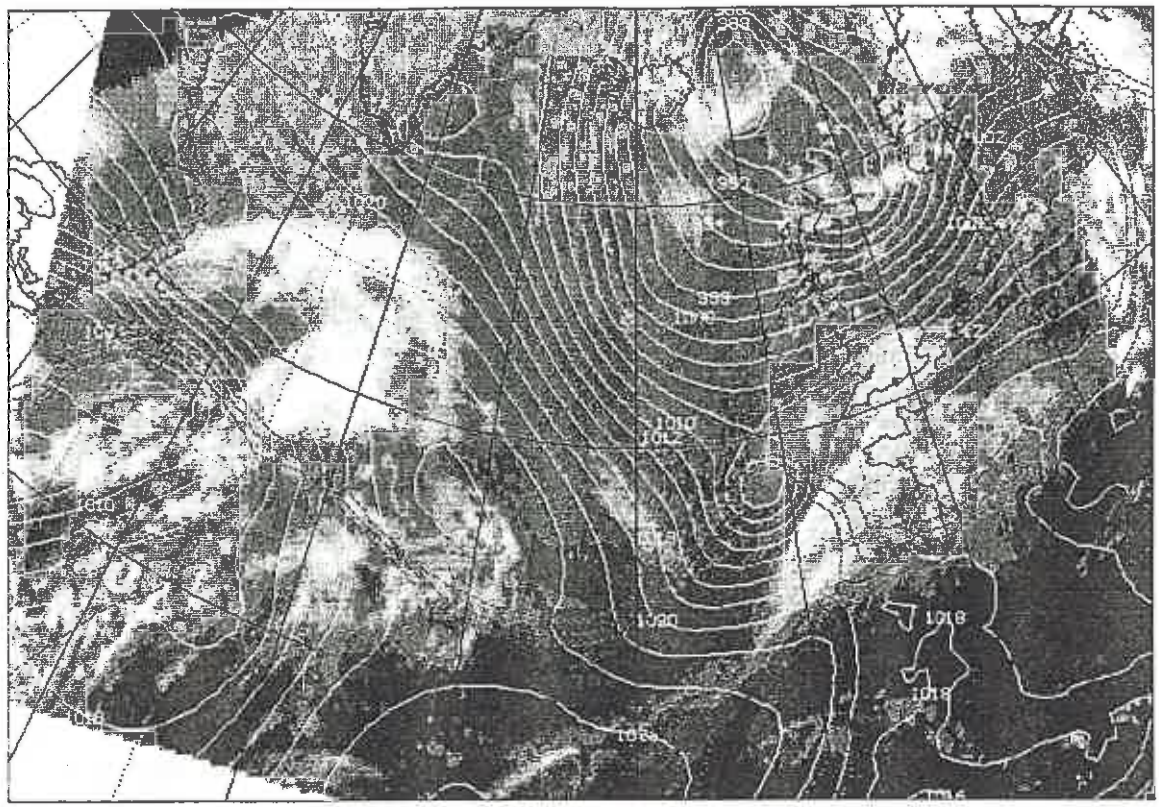

Figure 1. METEOSAT infrared satellite image for 18UT on 27th April 1992. Overlaid are contours of pressure at mean sea level at intervals of 2 hPa, and 10C, 11C and 12C isopleths of wet bulb potential temperature at 800 hPa to indicate the main surface frontal zones. These are taken from a LAM forecast beginning at 12UT on 26th April 1992, as are all subsequent Figures.

divergence of the Q vector at a given level gives an inadequate representation of the actual vertical motion at that level.

The difficulty of visualising the net effect of a given forcing div Q is considerably eased by solving the omega equation numerically, as we illustrate below. With the speed of modern processors this can be done using relaxation code, but library subroutines are also readily available, and have been used here. This directly provides the vertical velocity, the quantity of interest, integrating over the small-scale cellular patterns of the forcing. The integration has the further advantage of reducing the sensitivity of diagnosed outputs to the smallest scales in the system. It should be noted that the general method has been used by a number of authors previously, notably the application to a dry channel model of a baroclinic development by Keyser, Schmidt and Duffy (1992). The main focus of the present work, however, is upon validation and application to atmospheric systems, with the inclusion of moist effects.

We use the quasigeostrophic omega equation (Durran and Snellman (1987))

$$\left(\sigma(p)\nabla_p^2 + f_0^2\frac{\partial^2}{\partial p^2}\right)\omega = -2\nabla.Q - \frac{1}{\rho_0\theta_0}\nabla_p^2 S \qquad (1)$$

where σ(p) is a static stability parameter, dependent upon pressure only, f_0 is the coriolis parameter and

ω = dp/dt. The heating rate term S associated with moist ascent and descent is also included (see Krishnamurti (1968)), and the equation was solved with homogeneous boundary conditions at 0 hPa and 1000 hPa.

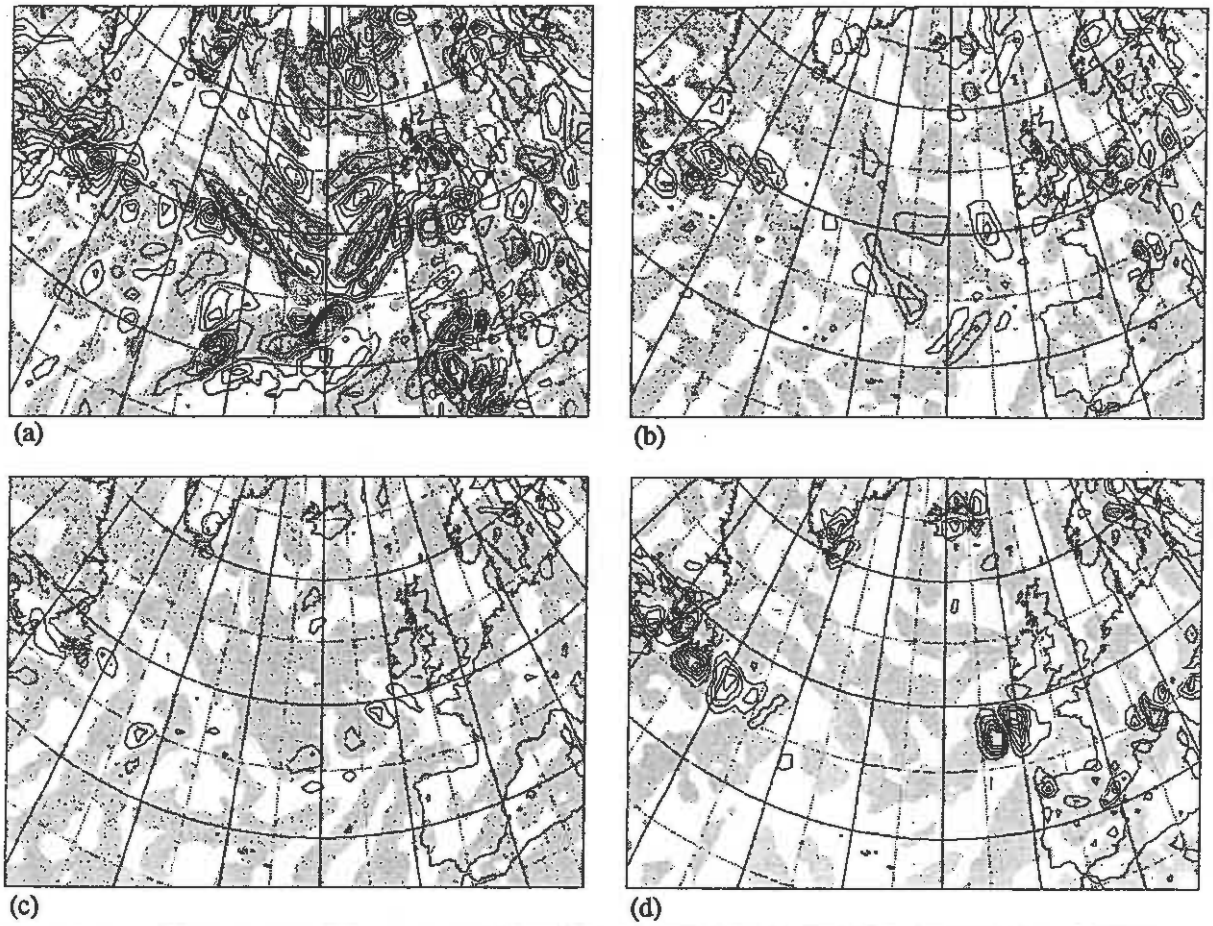

Figure 2. Divergence of Q vectors at (a) 300 hPa, (b) 500 hPa, (c) 700 hPa, (d) 900 hPa. Contours are at intervals of 10^{-17}m s^{-1} kg^{-1}. Positive (divergent) areas are shaded to coincide with the induced descent in later Figures.

Since σ is only dependent upon p Eq 1 is separable, and by defining a suitably stretched vertical coordinate (for example, $z = N/f_0\, z'$ where z' is the modified pressure coordinate of Hoskins' et al (1977)) it is readily transformed to the form of Poisson's equation :

$$\nabla^2 \omega = q \qquad (2)$$

where q is the forcing from Eq 1 or any individual part of it, and now the three-dimensional Laplacian operator is used. The influence of forcing at a point **r** due to each source point $\mathbf{r}_0$ is thus proportional to the Green's function $G(x,y,z|x_0,y_0,z_0)$ satisfying the boundary conditions (see eg. Morse and Feshbach (1953)), and thus inversely proportional to 3-dimensional distance in this space:

$$\omega = \iiint G(x,y,z \mid x_0,y_0,z_0)\; f(x_0,y_0,z_0)\, dx_0 dy_0 dz_0 \qquad (3)$$

where appropriate integration limits are chosen. In this quasigeostrophically scaled space, variations in the forcing (div Q) in the vertical are quite comparable to those in the horizontal within the troposphere where $N/f_0 \sim 100$. The div Q patterns in Fig 2 can be regarded simply as distributions of positive and negative charge, and the vertical motion as the induced field resulting from the sum of charges over the volume. The vertical velocity through much of the middle troposphere at least must be greatly influenced by the intense upper sources compared to rather weak internal sources.

(a)

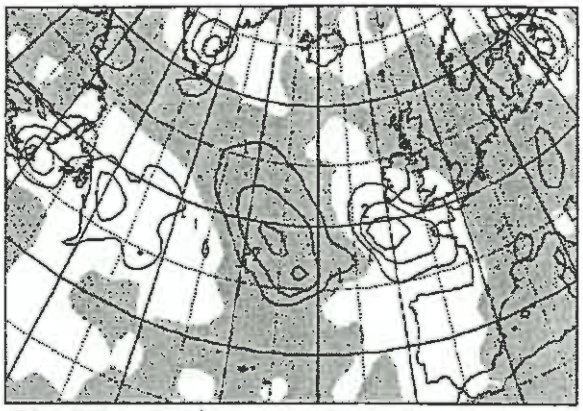

(b)

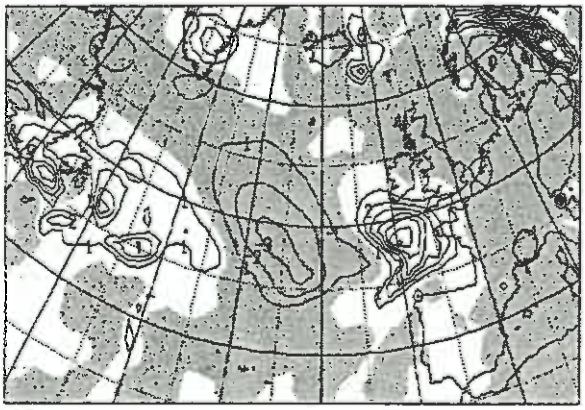

(c)

Figure 3. (a) Vertical velocity at 700 hPa, (b) solution to the omega equation at 700 hPa with only geostrophic forcing from all levels, (c) solution to the omega equation at 700 hPa with both geostrophic and diabatic forcing from all levels calculated as in the text. All have been converted to cm s^{-1} with contour interval 1 cm s^{-1}. Descent (negative values) is shaded.

Note that in practice because of the simplicity of the coordinate stretch it is not essential for most purposes to carry out the above transformations explicitly, but to note that they provide a conceptual basis for interpretation.

3. APPLICATION TO A MODEL

The omega equation was numerically solved as above using fields extracted from the Limited Area (LAM) version of the UK Meteorological Office's Unified Model (Cullen (1993). In this case the geostrophic wind and other fields were extracted on a 101.6km polar stereographic grid for the area shown, at 100 hPa intervals from 1000 hPa to 100 hPa. The value of $\sigma(p)$ used was determined by taking at each level the mean over the model grid at that level. The diabatic heating S has been approximated by adding in the grid-scale moist ascent/descent term (Vincent et al, 1978). At relative humidity greater than 85% (the model threshold for cloud formation) we have assumed this to be non-zero in ascent, and also in descent for ice, which sublimates rapidly.

Fig 3 shows the vertical velocity at 700 hPa from the forecast model and that deduced from the omega equation, both with and without diabatic forcing. Note that shading denotes negative values, ie. descent. In general the qualitative distribution of ascent and descent is reproduced in both cases. The descent is well described with only geostrophic forcing, except near 20W 40N in the base of the extending trough. The total geostrophic forcing only supports about 1/3 of the ascent in the warm sectors. The forcing due to latent heating is roughly equal to the geostrophic forcing in regions of ascent, and thus increases the total quasigeostrophic estimate to 2/3 of the actual ascent. Note that a very good description of the pattern on scales down to 200km or so is also reproduced, the most conspicuous qualitative difference being the underestimation of descent in the base of the trough.

Because solutions to either Eq 1 or Eq 2 are linearly superposable it is also straightforward to evaluate the vertical motion at a particular level (in this case 700 hPa is illustrated in Fig 4) induced by

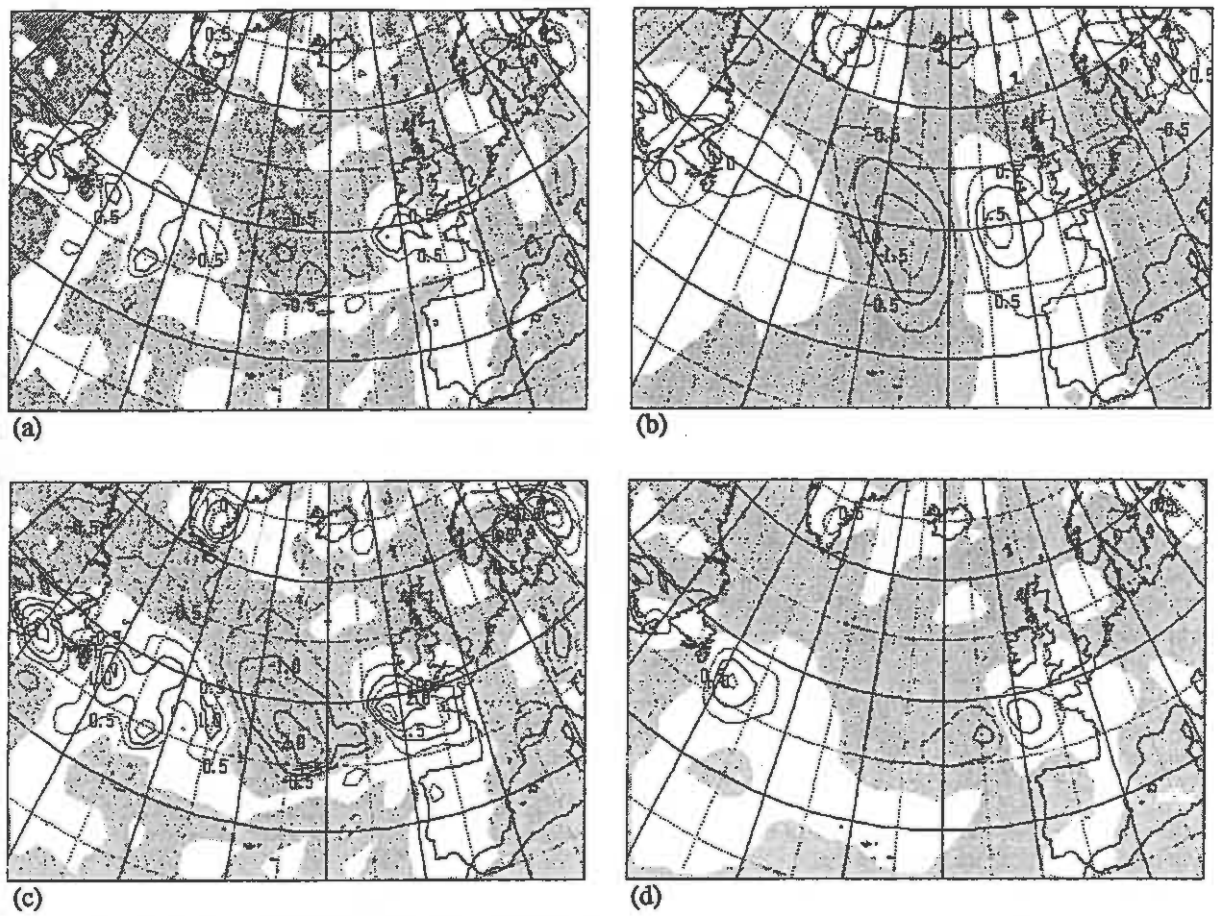

Figure 4. Solutions to the omega equation at 700 hPa with only geostrophic forcing at (a) 750-650 hPa, (b) 650-50 hPa, (c) 850-550 hPa, (d) 950-750 hPa. Units etc. as for Figure 3, 0.5 cm/s intermediate contours have been added.

a forcing process (for example the geostrophic forcing, diabatic forcing or total) in any other part of the fluid. This is achieved simply by integrating the omega equation for the entire domain with only the required forcing process in the appropriate part of the fluid included.

Fig 4 shows the vertical motion at 700 hPa induced by the geostrophic forcing (a) in the shallow 750-650 hPa layer, (c) the deeper 850-550 layer, (b) from upper levels (650-50hPa), or (d) from lower levels (950-750hPa). Consideration of these different selections of layers indicates several points about the dynamics of the system and the use of div Q:

1) The pattern of div Q at 700 hPa (Fig 2c) only very crudely describes the geostrophically induced or actual vertical motion.

2) Comparison of Figs 3(b) and 4(a) indicates that the motion forced by the div Q source at 700 hPa is, however, qualitatively similar in shape to the overall pattern of geostrophically forced vertical motion, though it does not predict even the correct sign of the vertical motion in the extending trough. Only a small fraction (perhaps 1/3) of the amplitude of the total geostrophically induced motion is present, and perhaps 1/10 of the actual ascent in the warm sectors.

3) From Fig 4(c) it can be seen that the 300hPa deep layer from 850-550 hPa induces most - about 2/3 - of the geostrophically forced vertical motion at 700 hPa.

4) Figs 4(b) and 4(d) contrast the dominant contribution of the upper levels to the main large-scale pattern with the small-scale dipolar forcing associated with the deformation of low level

temperature gradients. The ascent in the cloud head arises from both sources, though the upper level forcing of ascent is more closely collocated with the precipitation in the head region of the system. The pattern of the vertical motion forced from upper levels illustrates in part a far-field effect. The band of descent actually results from several parallel forcing bands at 300 hPa whose effects tend to merge into a single band with distance from the source; the vertical velocity itself shows two individual minima, which probably remain distinct because of local variations of static stability outside description by the quasigeostrophic approximation.

5) In the base of the trough at 20W 40N the forcing of descent due to the upper flow clearly dominates over the forcing of ascent in the shallower layer around 700mb. However, even this underestimates the actual vertical velocity, despite the lack of important diabatic sources in this region. The sources of this difference are being studied further.

4. CONCLUSIONS

To date the Q vector has been primarily used to study the intensifying stage of cyclones. The present study has been directed at 3-dimensional use of div Q to investigate the forcing of development from both upper and lower levels. It was shown that integrating the omega equation with forcing given by div Q and approximate latent heating rates is a practical and useful tool for this purpose with significant advantages over the use of div Q alone, including the ability to validate predictions against the forecast model vertical velocity.

Further, it was found that applying the concepts of electrostatic theory to the interpretation of the omega equation was informative and suggested useful working methods to attribute sources to the forcing of development, such as measures of "upper and lower level forcing".

These comparisons, as earlier ones, indicate the limited quantitative validity of quasigeostrophic theory. Local variations of static stability compared to the domain average are a significant factor in this regard, particularly at pressure levels occupied by both the troposphere and stratosphere, an inherent limitation of quasigeostrophic theory.

However, in the context of the electrostatic source approach this approximation may be seen as modifying the distance from the source, so that the importance of sources may be under- or over-estimated in ways which can be visualised and possibly corrected. Some of our results (not illustrated) suggest that other dynamical factors are also of some importance; these are being investigated further and will be discussed.

REFERENCES

Bishop, C. and A.J. Thorpe, 1994: Potential vorticity and the electrostatic analogy. *Quart. J.R.Meteor.Soc.*,**120**, In press.

Cullen, M.J.P., 1993: The Unified Forecast/Climate Model. *Meteor.Mag*, **122**, 81-94.

Durran, D.R., and L.W. Snellman, 1987: The diagnosis of synoptic-scale vertical motion in an operational environment. *Weather and Forecasting*, **2**, 17-31.

Hewson, T.D., ed., 1993: The Fronts 92 Experiment: a quicklook atlas. *JCMM Int. Report No. 15*.

Hoskins, B.J., I. Draghici and H.C. Davies, 1978: A new look at the ω-equation. *Quart.J.R.Meteor. Soc.*,**104**,31-38.

Keyser, D., B.D. Schmidt and D.G. Duffy, 1992: Quasigeostrophic diagnosis of three-dimensional ageostrophic circulations in an idealized baroclinic disturbance. *Mon. Wea. Rev.*, **120**, 698-730.

Krishnamurti, T.N., 1968: A diagnostic balance model for studies of weather systems of low and high latitudes, Rossby number less than 1. *Mon. Wea. Rev.*, **96**, 197-207.

Morse, P.M., and H. Feshbach, 1953: *Methods of Theoretical Physics*, McGraw Hill & Co., New York..

Vincent D.G., G.B. Pont and H. J. Edmon, Jr, 1977: Generation of available potential energy of an extratropical cyclone system. *Mon.Wea.Rev.*, **105**, 1252-1265.

MESOSCALE STRUCTURE AND LIFE CYCLE OF A POLAR LOW

G. C. Craig*, T. D. Hewson*, and C. Claud†

*Joint Centre for Mesoscale Meteorology, University of Reading,
†Laboratoire de Météorologie Dynamique du C.N.R.S., École Polytechnique

1. INTRODUCTION

Although polar lows have been the subject of numerous investigations over the past decade, many questions about their structure and formation remain unanswered, often the same questions as are raised in regard to larger-scale synoptic cyclones. Among these are the relative importance of baroclinic and barotropic instability and diabatic heating in the growth of the systems, the role of finite-amplitude upper level forcing in their initiation, and the influence of environmental factors such as sea surface temperatures and large-scale deformation fields.

In the case of polar lows, which are rarely well-resolved by the conventional data network, it has proved particularly difficult to address these questions. The principal source of information is frequently from satellites. However, it can be difficult to interpret remote sensing data in the absence of "ground truth", and basic questions about the structure of polar lows remain, regarding for example, the existence of fronts, and the organization of convective and other precipitation.

Here a case study will be presented, combining a variety of satellite-derived products with radar and conventional synoptic data. This case provided a particularly good opportunity for analysis due to the presence of a dense network of surface observations located on small islands and oil platforms in the seas around Scotland, that gave mesoscale resolution while the polar low was over water. In addition to considering some of the outstanding questions regarding polar lows for an individual system, it is hoped that this comparison of conventional and remote sensing data will be of benefit in the analysis of cases when fewer data sources are available.

2. SYNOPTIC ENVIRONMENT

The polar low to be described here was one of several that formed in a cold air outbreak on the western flank of an intense synoptic cyclone. At 12 UTC, 12 March 1992, this cyclone was centred off the coast of Norway, with the leading edge of the cold air mass trailing across the northern edge of Europe (Fig. 1). Within the cold air, a convergence zone was located between Iceland and northern Scotland, marked by straight band of convective cloud (Fig. 2). This band of cloud persisted for approximately 24 hours, until it was broken up by a sequence of small scale disturbances (the polar low labelled A in Figs. 1 and 2 propagated out of the region rapidly, leaving only the straight cloud band).

The satellite image in Fig. 3, from 1305 UTC, 14 March, shows the mature structure of the final two disturbances which formed along the convergence zone. It is the second of these, centred just north of Scotland, which will be discussed in subsequent sections.

The 1000-500 mb thickness pattern (Fig. 4) shows there is substantial baroclinicity through the depth of the troposphere in this region, which is associated with a strong upper tropospheric jet, although the low-level winds shears are more modest. This figure also shows the extreme temperatures in the cold air mass, leading to an air-sea temperature difference of 5-10 K, which in turn produces strong diabatic heating. Together these factors indicate that the region is likely to be unstable to a combined baroclinic-barotropic instability, with diabatic heating augmenting the low-level thermal advection. Such instabilities have been studied theoretically by numerous authors (see Craig and Cho 1992 and refs.).

The absence of waves along the baroclinic zone prior to the afternoon of 13 March may be due an imposed deformation field. An analysis following the method of Bishop (1994) showed that the deformation

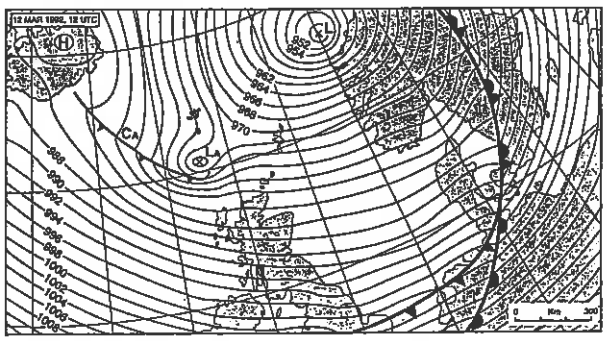

Figure 1. Surface pressure analysis for 12 UTC, 12 March 1992. Convergence zone is denoted by C_A.

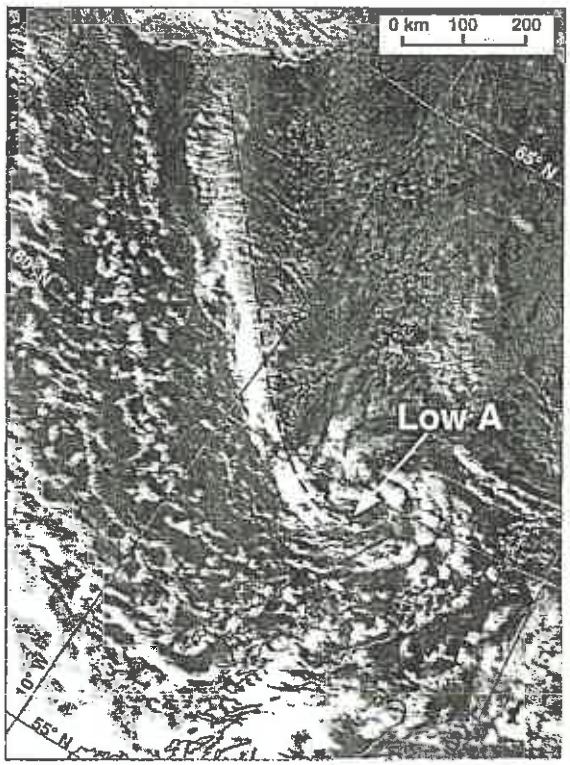

Figure 2. Infrared image for 1215 UTC, 12 March 1992. The coast of Iceland appears at the top of the picture, while Scotland appears at the bottom centre. (Courtesy of University of Dundee.)

induced by the large-scale flow was three times as great on the morning of 13 March as it was a day later when the polar low formed.

3. INITIATION

The polar low was first visible on satellite images as a wave on the cloud band immediately in the lee of Iceland. The operational model analysis at this time was misleading, the most notable error being the presence of a large amplitude upper-level short wave over Iceland. In the subsequent forecasts, this spurious feature led to a low-level development which was much more intense than observed, and wrongly located. While there is almost no radiosonde data in this region, a number of remote sensing products (TOMS and TOVS total column ozone, TOVS temperature retrievals, Meteosat water vapour images) showed little evidence of an intense pre-existing short wave.

On the contrary, the disturbance at upper levels appeared to develop at the same time as, or later than, the surface low. Figures 5 and 6 show the temperature in

Figure 3. Infrared image for 1305 UTC, 14 March 1992. Scotland and England appear on the left of the picture. (Courtesy of University of Dundee.)

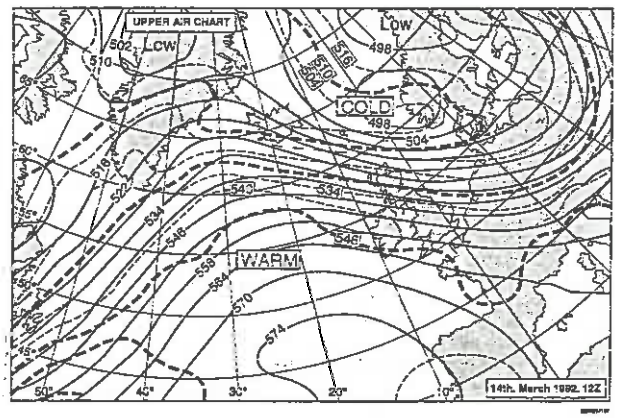

Figure 4. U.K. Met. Office global model analysis of 500 mb geopotential height (solid lines), and 1000-500 mb thickness (dashed lines), for 12 UTC, 14 March 1992.

the lower stratosphere, as derived from TOVS HIRS-2 and MSU sounders (Claud et al. 1992). Warm values will indicate a depression of the tropopause associated with a positive potential vorticity anomaly on isentropic surfaces. Early in the development of the polar low, there is relatively little indication of a warm anomaly

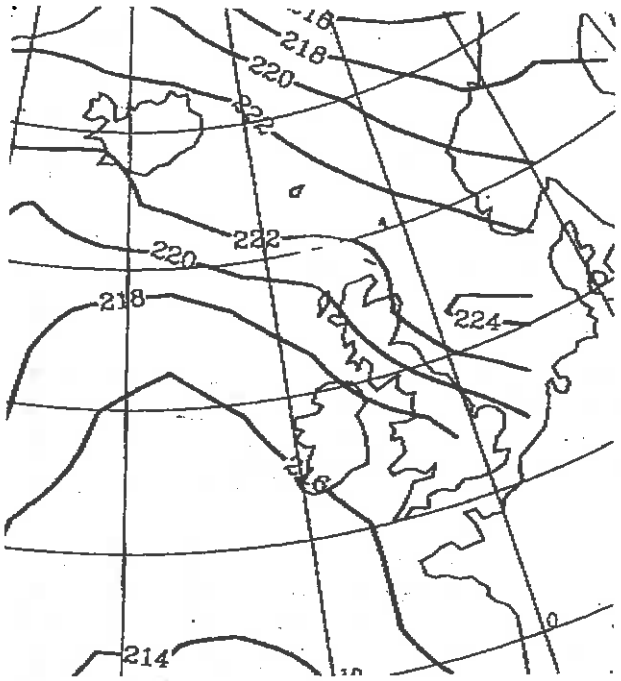

Figure 5. TOVS lower stratospheric temperature (K) (mean temperature in 222-380 mb layer), for 0447 UTC, 14 March 1992.

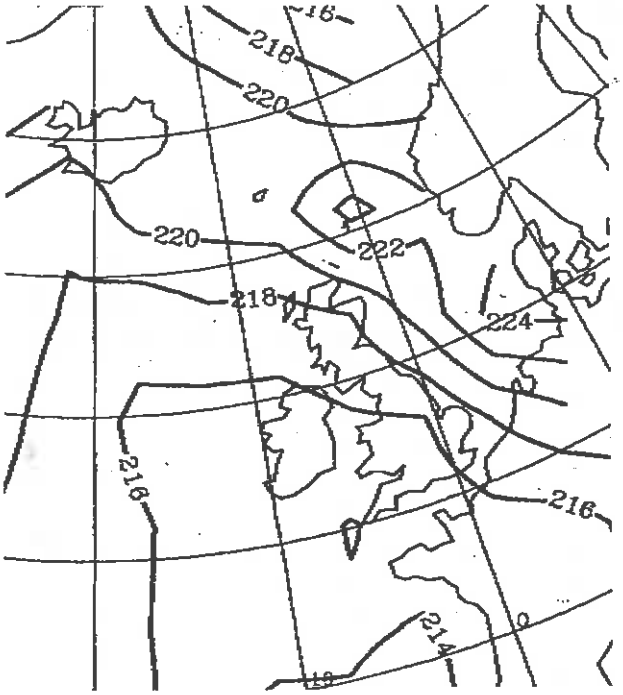

Figure 6. TOVS lower stratospheric temperature (K) for 1436 UTC, 14 March 1992.

(Fig. 5), whereas ten hours later, the upper level feature is quite pronounced (Fig. 6).

The most likely trigger for the growth of the polar low is Iceland, either by perturbation of the low-level flow, or local enhancement of the low-level baroclinicity due to differential heating between land and sea. The latter effect increased just prior to the formation of the low, due to a change in the direction of the large-scale flow. It should be noted that the initial perturbation need not have been large. A simple saturation estimate indicates that a baroclinic instability could have grown to maturity within 12 hours from an initial temperature perturbation of less than 1 K.

4. STRUCTURE OF MATURE POLAR LOW

Among the features visible in satellite imagery of the mature polar low (Fig. 3) are: a band of convective cloud extending to the southeast, eventually connecting to the cloud mass of another polar low; a cirrus cloud shield to the northeast of the low centre, curving across over the Shetland Islands; clear sky at the centre of the system; and low-level convection to the south and west of the system.

A careful analysis of surface observations at this time resulted in the chart shown in Fig. 7. The fronts drawn in this figure correspond to coherent bands of convection, as seen on radar, and are marked by large wind shifts,and small surface temperature gradients.

Convection occurs at the fronts and in the warm sector, however the greatest precipitation reached the surface under the cloud shield to the northeast. Here, the smooth appearance of the cloud suggests that convec-

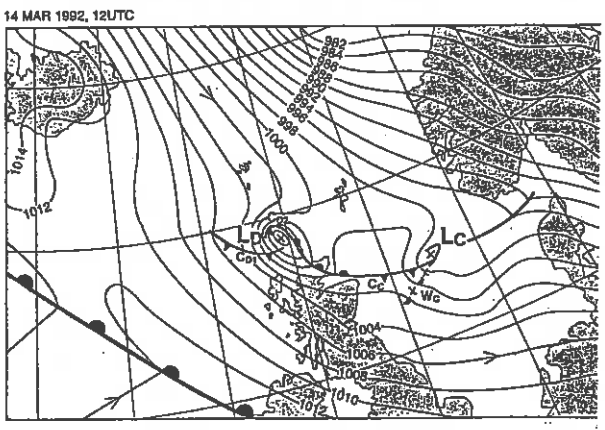

Figure 7. Surface pressure analysis for 12 UTC, 14 March 1992.

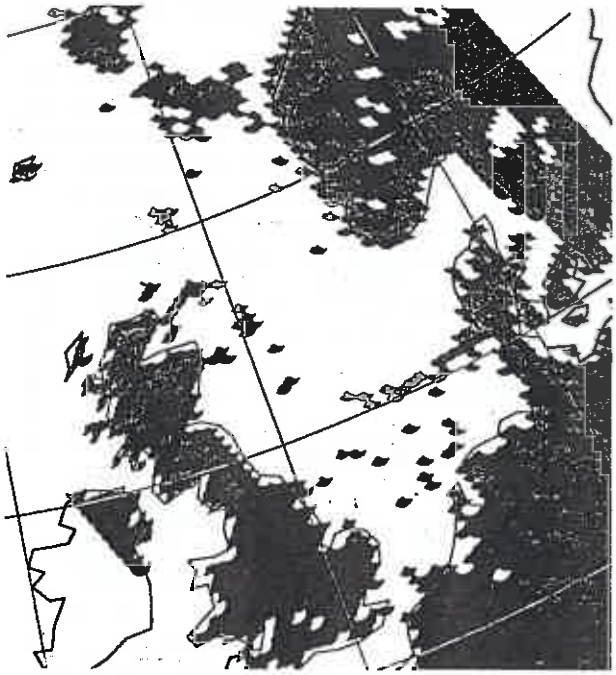

Figure 8. SSMI scattering index for 1551 UTC, 14 March 1992. Positive values are shaded. Note that signal over land may be due to contamination, for example by surface snow cover.

tion was not occurring. This is demonstrated more clearly in Fig. 8, a plot of an index of scattering by large ice particles above the freezing level, derived from SSM/I 85-GHz brightness temperatures (Claud et al. 1993). This index responds to large precipitation particles such as are found in convective cells. Fig. 8 shows the frontal convection, but no signal from the region of the cloud shield (Note that Fig. 8 is at a slightly later time than Figs. 3 and 7). Available upper-air data suggests that the atmosphere in this region is at or near a state of saturated slantwise neutrality, although this conclusion is difficult to confirm.

Fig. 9 shows a surface temperature analysis constructed from hourly observations from seven stations, shifted in space according to the track of the polar low. Warm temperatures are found in the core of the system, with the strongest gradients on the front to the north of the centre. The warm core is probably due to surface fluxes, as the air flow at this and previous times indicates that it is unlikely that such warm air could have been advected into the centre of the system.

5. CONCLUSIONS

As with many polar lows, the system described here appears to result from a combination of dynamical

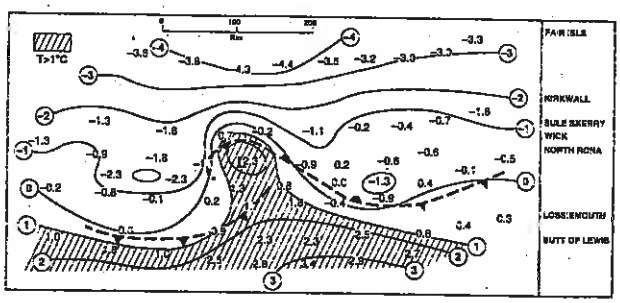

Figure 9. Surface temperature analysis constructed using data from 09 UTC to 17 UTC, 14 March 1992, at the stations listed on the right of the figure. Position of fronts taken from 12 UTC surface analysis.

(baroclinic and barotropic) instability and diabatic heating. Unusually, it appears to form without significant upper-level support. The dramatic development occurring in forecasts initialized with the spurious upper-level wave present is interesting, since it suggests that had such a feature been present in reality, it would have dominated the subsequent evolution.

Despite the presence of a warm core, the mesoscale structure of the polar low is more reminiscent of midlatitude maritime cyclones than more convective systems such as tropical cyclones. Similar features include a stratiform cloud head, and warm and cold fronts, with the strongest temperature gradients found on the front bent back around the low centre.

REFERENCES

Bishop, C. H. , 1994: Domain independent attribution and its value in the verification of dynamical theories of frontal waves and frontogenesis. *J. Atmos. Sci.* (submitted).

Claud, C., N. A. Scott, and A. Chedin, 1992: Use of TOVS observations for the study of polar and arctic lows. *Int. J. Remote Sens.*, **13(1)**, 129-139.

Claud, C., N. M. Mognard, K. B. Katsaros, A. Chedin, and N. A. Scott, 1993: Satellite observations of a polar low over the Norwegian Sea by Special Sensor Microwave Imager, Geosat, and TIROS-N Operational Vertical Sounder. *J. Geophys. Res.*, **98(C8)**, 14,487-14,506.

Craig, G. C., and H.-R. Cho, 1992: A study of two cases of comma cloud cyclogenesis using a semigeostrophic model. *Mon. Wea. Rev.*, **120**, 2943-2961.

DYNAMICS OF MESOSCALE SUB-STRUCTURE AT FRONTS

by

Alan J Thorpe

JCMM, Dept of Meteorology
University of Reading
Reading, England

1. INTRODUCTION

The mathematical theory of frontogenesis (Hoskins 1982) gives a consistent description of the dynamics of two-dimensional frontal zones in which geostrophic balance is imposed on the along-front wind. This semi-geostrophic theory filters all inertia-gravity waves and their related instabilities. Despite these restrictions it is able to describe many fundamental dynamical aspects of fronts such as the process of frontogenesis and the cross-frontal circulation.

Atmospheric fronts also exhibit a wide range of sub-structures which can loosely be called mesoscale. These include:

frontal wave cyclones
frontal rain and snowbands
line convection including segmentation
wave-clouds

Many of these cannot be described by the semi-geostrophic theory due to the filtering mentioned previously. Others such as secondary wave cyclones are three-dimensional structures which are clearly not described in two-dimensional theory but which are of a sufficiently large horizontal scale that the balanced flow assumption may be applicable. It is the aim in this review to discuss the dynamics of two of these phenomena: frontal wave cyclones and frontal rainbands. These are not especially related sub-structures but they are examples of a three and a two-dimensional phenomenon respectively.

From a theoretical viewpoint the most insightful approach to describe the dynamics of these systems is via what has become known as PV-thinking. It is reaffirmed here that the phenomena in question cannot be fully understood without consideration of the potential vorticity. It has been argued that PV-thinking does not give any new insight over-and-above that available from previously used principles not involving PV. There is no doubt that many processes in the physical world can be described equally well using alternative formulations. But the objective is to find the most succinct concept or set of concepts that explain the essential features. For the phenomenon discussed here PV does indeed give this "maximally simple but sufficiently complete" description.

2. THEORETICAL CONCEPTS

2.1 PV thinking

For many applications of PV ideas on the mesoscale then the flow is neither dry adibatic nor frictionless so that the PV is not conserved. The PV evolution equation is:

$$\frac{DPV}{Dt} = \frac{1}{\rho} \nabla.(\underset{\sim}{\zeta} \dot{\theta} + \theta \nabla \times \underline{F})$$

$$PV = \frac{1}{\rho} \underset{\sim}{\zeta} . \nabla \theta \qquad \text{if} \quad \frac{D\theta}{Dt} = \dot{\theta}$$

and $\underline{F}$ is the frictional force. A simplification arises if the flow is saturated adiabatic and frictionless i.e.

$$PV_e = \frac{1}{\rho} \underset{\sim}{\zeta} . \nabla \theta_e \qquad \text{and} \quad \frac{DPV_e}{Dt} = 0$$

$$\text{if} \quad \frac{D\theta_e}{Dt} = 0 \quad \& \quad \underline{F} = 0$$

where θ_e is the equivalent potential temperature and PV_e is the equivalent potential vorticity.

These equations imply that in mesoscale systems we do not expect PV to be conserved and

further that latent heat release will be associated with a dipole of PV anomalies with positive below and negative above the zone of maximum heating. The question then arises as to whether PV remains as a useful quantity in such cases. For some systems with a degree of balance, possibly involving non-linear balance, the answer seems to be in the affirmative.

2.2 Instability

The potential vorticity is also involved in certain instability criteria. These criteria arise by consideration of a balanced stationary basic flow in which an infinitesinal perturbation is implanted. The tendency of the perturbation to grow in time, with constant shape, can then be found mathematically. It is important to remember that the stability of the flow is, in the classical analysis, dependent only on the properties of the basic state. The question such stability analyses answer is which aspect of the basic flow indicates its stability?

In the case of the two mesoscale sub-structures to be described here that property of the basic flow is its potential vorticity. In other words without a knowledge of the potential vorticity of the flow one could not assess its susceptibility to perturbation. This indicates the fundamentality of the PV viewpoint.

For a general geostrophically-balanced basic state instability depends on either the existence of extrema of PV or on the absolute sign of PV relative to the sign of the Coriolis parameter. We postpone discussion of these criteria to the following sections.

3. FRONTAL WAVE CYCLONES

2.1 Observations

As is well-known the Bergen school formulated a concept of a semi-permanent polar front along which cyclone families would form and propagate. From a theoretical viewpoint a fundamental aspect of this model is the existence of a special environment in which the cyclones form. The observational basis for the Bergen picture was at that time limited. Theoretical ideas subsequent to the development of this model moved attention away from the polar front concept. Baroclinic instability, in its archetypal form, involves an instability of the broad baroclinic climatological zonal flow. The developing cyclones are of synoptic scale and produce, during their life-cycle, zones of stretching and shearing deformation leading to frontogenesis.

It is the contention here that these frontal zones spawn secondary wave cyclones which are typically of a much smaller horizontal scale than the parent cyclone. It is proposed here that these secondary mesoscale sytems are the cyclones described so eloquently by Bjerknes and colleagues.

It is worth asking whether there is good observational evidence for these secondaries and by inference for the Norwegian picture given improvements in the observational base. Elsewhere in these conference proceedings Ayrault et al 1994 give results from a study of an objectively determined evaluation of very-high frequency variability in the Atlantic storm-track. This is in an attempt to differentiate storms into larger longer-lived storms which explain variability on the 2 to 5 day time-scale and the smaller short-lived ones which occur in the 1 to 2 day frequency range. It is this latter category which involve the secondary waves having a horizontal scale of 1000km or less.

Here we discuss on the subjective evidence from operational surface charts. Current practise in drawing surface charts over oceanic regions is, in this context, worth commenting on. The bench forecaster has many data available as he or she constructs a surface analysis including NWP first guess fields, satellite imagery, satellite soundings, merchant ship surface and upper-air, air-reps, buoys etc. This represents an inadequate data-base but does mean that the forecaster will only include structures if evidence exists.

During the recent FRONTS 92 experiment an analysis was performed by Tim Hewson of the JCMM of the occurrence on surface charts of secondary wave cyclones. In keeping with the theoretical requirement to evaluate the environment in which these systems develop a classification scheme was used which identified 5 types of secondary wave cyclones dependent on their location relative to the parent cyclone.

The charts used were for March, April, and May 1992 at 12Z in the north Atlantic sector. Evidence of the wave was required on 2 consecutive charts and the intermediate 6-hourly charts were checked for consistency. The definition of a frontal wave adopted concerned the local structure of the front: moving along the front it must rotate in a clockwise direction and/or the vorticity have a local maximum. The wave type was classified according to the surrounding synoptic environment at the time of its appearance on the chart.

It was found that on average 1 wave appeared somewhere in the region per day and that 50% of these were developmental. As shown below, in a hypothetical surface analysis, there appeared to be 5 distinct types. These, together with the number of events in the 3-month period and the percentage which were developmental, were:

(i) cold air trough (15, 67%)
(ii) cold front wave (25, 48%)
(iii) warm front wave (9, 11%)
(iv) col wave (16, 63%)
(v) warm sector wave (9, 11%)

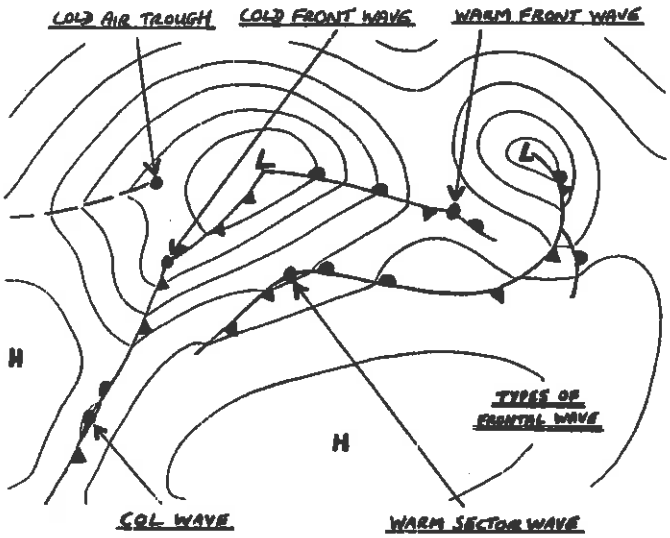

Figure 1: Schematic surface analysis showing the various categories of frontal wave cyclones found by Hewson.

It was found that col waves were more developmental than cold frontal waves and furthermore development is more pronounced ahead of a confluent upper trough. Col waves also account for many major storms in the north-east Atlantic such as on 16/10/87, 11/4/89, 21/1/90, and 2/2/90. The IOP3 case of FRONTS 92 (Hewson 1993) on 27/4/92 also falls into this category.

In conclusion there is strong evidence for a class of cyclones which develop on pre-existing tight frontal zones. We refer to these as frontal wave cyclones and often they occur as a secondary development on the fronts formed within a parent cyclone. Such cyclones consequently occur at the end of the storm-track. These are often of a short horizontal scale putting them in the mesoscale category. They can be developmental but often are not. From a theoretical viewpoint certain critical questions arise from the observational evidence:

Do these cyclones develop from the same or different mechanisms from the parent cyclones?

Why are some frontal wave cyclones developmental whilst others are not?

What is the importance of upper versus lower level forcing?

3.2 Development mechanisms

The various scenarios for the development of cyclonic storms in mid-latitudes can be summarised by the interaction of so-called Rossby or edge waves. These Rossby waves can exist at a potential vorticity gradient or at a potential temperature gradient as measured along a material surface. Such a material surface might be an isentropic surface or an iso-PV surface, such as the tropopause, respectively or the Earth's surface in either case. Ordinarily such a Rossby wave is neutral involving no development. A synoptic example might be an upper-level propagating short-wave trough.

Baroclinic and/or barotropic instability involves the mutual interaction of 2 edge waves allowing wave growth to occur. The term instability is being used here in its loosest sense to mean an increase in amplitude; it is not necessary to make any supposition about constant shape-exponential growth as in the normal mode. Arguments about normal mode versus initial value growth confuse the fact that Rossby wave interaction is the common factor.

The classic baroclinic instability model of Eady encapsulates the mutual interaction of a Rossby wave on the tropopause thermal gradient and a Rossby wave on a surface baroclinic zone. In general the interaction between 2 edge waves will occur only if they are close enough to one another. For horizontal interaction this means that they must have a separation less than or of order the horizontal wavelength of the wave. The same applies in the vertical but with the vertical distance having been scaled with N/f.

The archetype for barotropic interaction features 2 Rossby waves on the edges of a horizontally-oriented PV strip. This has been discussed in the context of a horizontal-shear forced front by Joly and Thorpe 1990. In an equivalent way horizontal interaction can occur at the ground if there is a extremum of potential temperature, see Schär and Davies 1990.

Here we will explore the vertical and horizontal interaction mechanisms with particular reference to end-of-stormtrack fronts as the basic flow environment for the development.

Consider a mature frontal zone in which there has been a period of frontogenesis leading to a tight frontal gradient. The role of moisture and friction is to produce a lower-tropospheric strip of high potential vorticity lying along the front. Observational evidence for this strip comes from the FRONTS 87 campaign, see Thorpe and Clough 1991 and the figure shown here. Theoretical evidence for its existence can be found in Thorpe and Emanuel 1985 (moist processes) and Cooper et al 1992 (frictional processes).

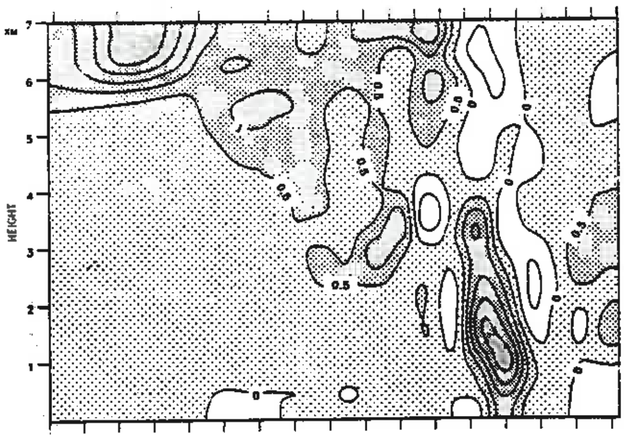

Figure 2: Vertical cross-section through the IOP8 cold front of FRONTS 87 showing the PV distribution; from Thorpe and Clough 1991. The contour interval is 0.5 PVU and ticks on the horizontal axis are 50 km apart whilst those on the vertical axis are 1 km apart. The surface cold front is immediately to the west of the lower tropospheric PV maximum.

Given the geostrophic flow and temperature of such a front one can perform a traditional stability analysis. This requires, for normal modes to be found, that the frontogenesis be assumed to have ceased. This is a plausible assumption for an end-of-stormtrack front but in section 3.4 we also consider the role of active frontogenesis. In Joly and Thorpe 1990 the basic state chosen was taken from the front produced during a moist two-dimensional Eady wave development; this had previously been discussed by Emanuel et al 1987. The growth rate curve is given below in figure 3.

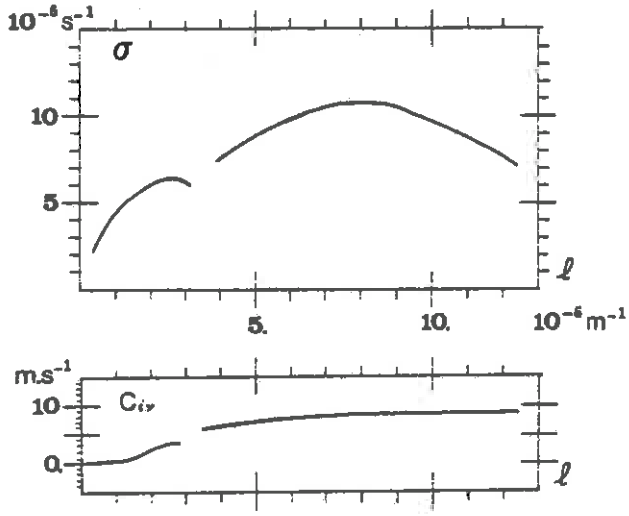

Figure 3: Growth rate and along-front phase speed as functions of the along-front wavenumber; from Joly and Thorpe 1990. The maximum growing wave has a horizontal scale of 800 km with a growth rate of just less than 1 day.

This study showed that a new family of frontal waves exist at wavelengths of order 800 km associated not with upper-jets but with lower-level jets. These waves have structure that is more surface confined than classical baroclinic waves. The new modes derive a significant part, but not all, of their energy from the frontal horizontal shear via barotropic conversion. If waves have a greater horizontal scale then they also use the baroclinic conversion. The key feature of these waves is that they depend on the presence at the front of anomalies of potential vorticity (or equivalently potential temperature). This is, in turn, the result of the effects of diabatic processes in the past history of the front.

3.3 Non-linear structure

The low-level instability of the frontal potential vorticity strip has been studied into the non-linear regime by Malardel et al 1993. They found that there is a vortex roll-up as shown here in figure 4. The initial line of PV becomes distorted into a series of more-or-less circular vortices.

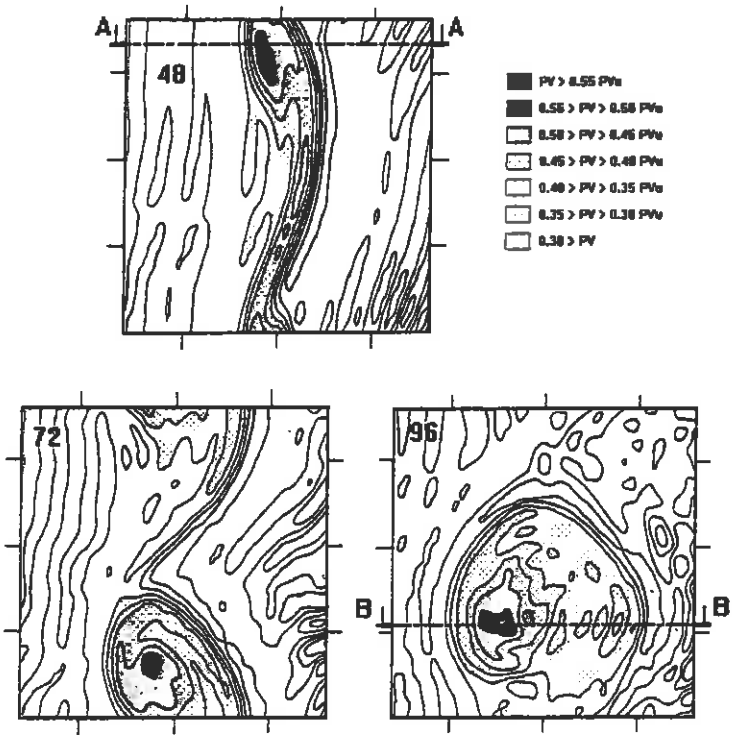

Figure 4: Evolution of the surface potential vorticity associated with frontal wave instability; from Malardel et al 1993. this shows the distortion of the initial two-dimensional PV strip into vortices.

There is only a small pressure deepening associated with such development. This is an extremely significant aspect showing that although such instability can account for waves at fronts it cannot typically account for significant development in the pressure field. Many frontal wave cyclones are not developmental (about 50% from the subjective climatology quoted earlier) so this finding is relevant. Forecasters are probably not used to looking for such vortices because of thier weak signature in the pressure field.

3.4 Upper-level forcing

PV ideas suggest that to allow cyclones to draw on the amply supply of potential energy stored at frontsthere needs to be significant vertical interaction. this can only occur if the horizontal wavelength of the wave is sufficiently long. Thorncroft and Hoskins 1990 have given an example in an idealised baroclinic life-cycle simulation of the interaction of an upper level PV anomaly, associated with a tropopause trough, with a surface front; see figure 5. The resulting isolated frontal wave cyclone achieved a pressure drop of order 10 mb.

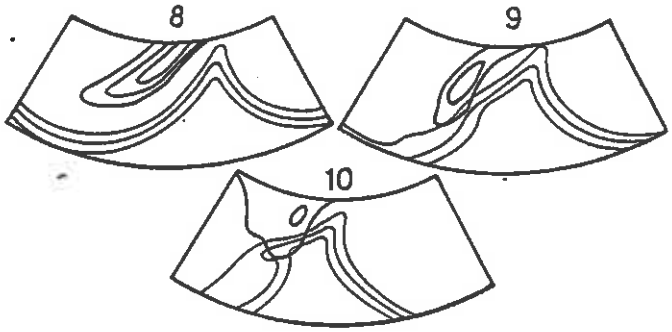

Figure 5: Frontal wave development in an idealised life-cycle experiment from Thorncroft and Hoskins 1990. Thinner solid lines are surface θ whilst bolder lines are PV contours on the 330K surface. The numbers are days since the integration began. This shows clearly the upper-lower level interaction.

This result is significant and shows that one might be able to propose a simple differentiation of frontal wave cyclones into the following 2 categories:

type D - developmental, requiring upper-level PV anomalies interacting with a surface front; large space (> 1000 km) and time (> 1 day) scales

type ND - non-developmental, requiring a lower tropospheric frontal PV anomaly lying along the front; short space (< 1000 km) and time (< 1 day) scales

The term developmental is being used here to refer only to the pressure-deepening - type ND can, for example, involve significant increases in across-front wind as the vortices form. The term "ordinary" frontal wave has been coined by Malardel et al 1993 for type ND. The above constitutes an hypothesis which can be tested from appropriate field observations as well as providing a forecasting rule of some significance.

Extension of these ideas to arbitrary intial-value type perturbations has recently been studied and reported elsewhere in these proceedings, by Joly 1994.

3.5 Role of deformation

For frontal waves growing at a pre-existing front an important question is what effect any larger-scale frontogenetic forcing has on the wave. Frontogenesis (or frontolysis) is due to shearing and/or stretching deformation and, of course, leads to an intensification of the front. For theoretical analysis of frontal waves this means that the frontal flow, whose stability is being examined, is not stationary in time. This means that simple normal mode type instability calculations are not applicable.

In Joly and Thorpe 1991 the case of pure shearing deformation was studied in the context of the Eady basic state. They found that such frontogenesis actually enhanced the instability although much less so than the inclusion of latent heating. The technique used was a version of the so-called linear tangent-resolvent matrix method.

On the other hand stretching deformation might be expected to have a deleterious effect on incipient waves because of factors like the compression of waves in the across-front direction and stretching in the along-front direction. Therefore in this case there are no constant shape normal mode solutions possible. This problem has recently been studied by Bishop and Thorpe 1994 a and b. They found that a deformation rate in excess of f/4 prevents wave amplification. For strain rates greater than $0.6 \times 10^{-5}\ s^{-1}$ the model predicts that wave slope amplification greater than a factor e is impossible.

There are 2 further corollaries from this work. The first is that we need to find the stretching deformation rate at actual fronts in order to assess their propensity for wave development. This is not straightforward and an attempt to do this using the ideas of attribution described in Bishop and Thorpe 1994c are being made currently. The second is that such deformation acts to increase the potential for wave growth while the frontogenesis proceeds. Thiss can be released later, conceivably explosively, when the deformation ceases. The deformation prevents the waves but also acts to increase the likelihood of instability by narrowing and intensifying the frontal potential vorticity strip.

4. FRONTAL RAINBANDS

4.1 Conditional symmetric instability

Observations indicate that frontal precipitation is often organised into a series of bands parallel to fronts, see Matejka et al 1980 for details. The nature of frontal cloud processes has been studied for some time dating back at least as far as Kleinschmidt's early research (see Thorpe 1994 in this volume) with ideas of the possibility of an analogue to convective instability. Frontal precipitation is clearly rarely convective in origin given the observed vertical stability and low preciptation rates.

Ascent at fronts is shown in the theory of frontogenesis to be a consequence of frontogenesis itself. Condensation of water vapour in the frontal ascent will naturally lead to precipitation and this will, for example, appear in NWP models as so-called large-scale or dynamic precipitation. So one can ask what is the requirement for further explanation of frontal rain and snowfall. The main answer to this, historically, has been the requirement to explain the banded structure of the clouds as opposed to a broader region of nearly uniform ascent.

It has also been found recently from high-resolution frontal observations that certain structures exist in the wind and temperature fields which do not seem to be accounted for in the simplest theories of frontogenesis. An example of this is the observation that the frontal ascent is often characterised by absolute momentum (m) and equivalent potential temperature surfaces being parallel. The absolute momentum is proportional to the absolute angular momentum on an f-plane and is defined as $m = v + f x$ where v is the along-front wind and x is the across-front coordinate.

The theory of conditional symmetric insatability (CSI) dates from the work of Bennetts and Hoskins 1979 although various incomplete descriptions of the mechanisms involved had been given earlier by Solberg, Kleinschmidt, and Sawyer. The theory describes an instability of a two-dimensional geostrophic flow to perturbations oriented along that flow direction. There are various equivalent forms for the criterion that has to be satisfied by the basic state to exhibit the instability:

$$f\,PV_e < 0,\ R_e < f/\zeta,$$

$$f\,\zeta_{\theta e} < 0,\ (\partial \theta e/\partial z)_m < 0$$

where $\zeta_{\theta e}$ is the vorticity measured on an moist isentropic surface and R_e is the Richardson number based on the θe vertical gradient and the vertical shear of the basic flow. Note that the term CSI is reserved for motions which are moist convectively stable $(\partial \theta e/\partial z)_x > 0$ and inertially stable $f\,\zeta > 0$.

Parcel theory provides another way to assess instability. Then a direction must be specified along which the parcel is lifted. The linear theory suggests that typically parcel ascent is close to neutral bouyancy i.e. along the sloping θe surface:

$$\text{at neutral buoyancy: } f\,m'\,x' > 0$$

$$\text{along momentum surface: } g\,\frac{\theta'}{\theta_0}\,z' > 0$$

where prime indicates a difference between the parcel and its environment, and (x', z') is the parcel displacement in the x-z plane. If a cloud base and top has been established then the amount of so-called slantwise convective available potential energy is independent of the parcel path, see Emanuel 1983.

Evidence for the existence of CSI at fronts is now available from, for example, Emanuel 1988, Thorpe and Clough 1991, Lagouvardos et al 1993.

4.2 Non-linearity

The roll circulations deduced within the context of the linear theory have been described into the non-linear regime by using numerical simulations; see Thorpe and Rotunno 1989, Persson and Warner 1991, and Innocentini and Neto 1992. It is plausible to suppose that such circulations will over a period of time adjust the atmosphere to a near-neutral state such as is commonly observed.

4.3 Three-dimensional structure

An important aspect of the practical application of the theory of CSI to fronts is that observations show that rainbands are distinctly finite in length. This means that we need to assess the effects of the three-dimensional structure necessarily imposed by this finite length. This has recently been addressed by Jones and Thorpe 1992 who show that the (two-dimensional) theory of CSI may hold as long as the length of the rainband is longer than about twice the across-front wavelength of the rolls. For shorter bands the CSI growth is substantially reduced. They also found that the bands tend to be rotated anticyclonically relative to the front depending on the importance of viscous effects.

4.4 Role in frontogenesis and cyclogenesis

Another important factor is to determine the role of CSI on frontogenesis and cyclogenesis. This has beeen studied in the context of full numerical modelling studies, discussed in the next section, as well in more general terms. The semi-geostrophic theory of frontogenesis can be extended to incude the effects of latent heat release occuring in an atmosphere with effectively zero stability to slantwise ascent i.e. for $PVe \approx 0$. This has been reported for deformation frontogenesis by Thorpe and Emanuel 1985 and for horizontal shear frontogenesis, such as occurs in an Eady wave, by Emanuel et al 1987. These results show scale contraction of ascent and an increased growth rate of the front.

From a physical viewpoint this shows that the frontal environment is an ideal one for the feedback between latent heat release and frontogenesis. The parcel displacements favourable for CSI along the sloping front are exactly those produced by the cross-frontal circulation. In other words not only is the atmosphere unstable by also the "dry" dynamics of the front move parcels in just the right direction for releasing the potential energy.

A further question to be addressed is the

role of snow sublimation and rain evaporation from the precipitation bands. This has recently been considered by Parker and Thorpe 1994. They find that the effect on the geostrophic flow is minimal but there is a strong coupling to the ageostrophic motion leading to a cross-front elevated jet beneath the frontal surface.

4.5 Modelling studies

The use of high resolution cloud-models to describe frontal circulations in two-dimensions has taken place recently. Examples include Hsie et al 1984, Knight and Hobbs 1988, Bénard et al 1992 a and b, & Redelsperger and Lafore 1994. New features have emerged such as the important role of the frictional boundary layer in the potential vorticity budget of frontal zones. Alternative ideas about rainband dynamics are emerging involving the role of gravity waves organizing convection. Such studies are approaching the complete three-dimensional description of the cyclone with high resolution models including zones embedded at fronts resolving the mesoscale detail.

5. DISCUSSION

The mesoscale sub-structures described here - namely frontal wave cyclones and frontal rainbands - have been subject to theoretical study in the last few years. Hypotheses are emerging which need to be tested with high resolution field observations. They have, of course, been many such campaigns already focussing in the general area of mid-latitude cyclones. However there are several aspects for which almost no detailed mesoscale observations exist. These include the structure of the tropopause with particular reference to the potential vorticity. Also the data which are available tend to involve non-synchronous observations which can only be analysed via a space-time conversion. Therefore there is a need for simultaneous observation of a large mesoscale area in the cloudy zones of such cyclones.

The Fronts and Atlantic Storm Tracks Experiment, FASTEX, programme is attempting to address these questions. The motivation is not only to improve understanding but also to provide input to weather forecasting and climate issues. The secondary wave cyclones are responsible for much of the problems in forecasting for north-west Europe at the end of the Atlantic storm-track. They are also associated with major zones of cloudiness which impacts strongly via radiative processes onto the climate system.

From a theoretical viewpoint it is clear that the pioneering research of the Bergen school and also of the German-speaking community early in this century has been the springboard to the understanding of mid-latitude cyclones. Many of the components of the current picture were in place at that time but the modern era has allowed these pieces to be fitted together into a more complete and rigorous framework.

6. REFERENCES

Ayrault F, Lalaurette F, Joly A, and Jousselin C, 1994: On the track of European secondary cyclones. Bergen conf. pre-print volume.

Bénard P, Redelsperger J-L, and Lafore J-P, 1992a: Nonhydrostatic simulation of frontogenesis in a moist atmosphere. Part I: General description and narrow rainbands. J. Atmos. Sci., 49, 2200-2217.

Bénard P, Redelsperger J-L, and Lafore J-P, 1992b: Nonhydrostatic simulation of frontogenesis in a moist atmosphere. Part II: Moist potentail vorticity budget and wide rainbands. J. Atmos. Sci., 49, 2218-2235.

Bennetts D A and Hoskins B J, 1979: Conditional symmetric instability - a possible explanation for frontal rainbands. Q. J. R. Meteorol. Soc., 105, 945-962.

Bishop C H and Thorpe A J, 1994a: Frontal wave stability during moist deformation frontogenesis. Part 1: Linear wave stability. J.Atmos. Sci., 51, in press.

Bishop C H and Thorpe A J, 1994b: Frontal wave stability during moist deformation frontogenesis. Part 2: The suppression of non-linear development. J.Atmos. Sci., 51, in press.

Bishop C H and Thorpe A J, 1994c: Potential vorticity and the electrostatics analogy: quasi-geostrophic theory. Q. J. Meteorol. Soc., 120, April issue.

Cooper I M, Thorpe A J, and Bishop C H, 1992: The

role of diffusive effects on potential vorticity in fronts. Q. J. R. Meteorol. Soc., 118, 629-647.

Emanuel K A, 1983: The Lagrangian parcel dynamics of moist symmetric instability. J. Atmos. sci., 40, 2368-2376.

Emanuel K A, 1988: Observational evidence of slantwise adjustment. Mon. Wea. Rev., 116, 1805-1816.

Emanuel K A, Fantini M, and Thorpe A J, 1987: Baroclinic instability in an environment of small stability to slantwise moist convection, Part 1: Two-dimensional models. J. Atmos. Sci., 44, 1559-1573.

Hewson T, 1993: The FRONTS 92 Experiment: A Quicklook Atlas, JCMM Internal Report No. 15, available from the Joint Centre for Mesoscale Meteorology, University of Reading.

Hoskins B J, 1982: The mathematical theory of frontogenesis. Ann. Rev. Fluid Mech., 14, 131-151.

Hsie E Y and Anthes R A, 1984: Simulation of frontogenesis in a moist atmosphere using alternative parameterizations of condensation and precipitation. J. Atmos. Sci., 41, 2701-2716.

Innocentini V and Neto C, 1992: A numerical study of the role of humidity in the updraft driven by moist slantwise convection. J. Atmos. Sci., 49, 1092-1106.

Joly A, 1994: Linear and non-linear aspects of non-modal frontal waves. Bergen conf. pre-print volume.

Joly A and Thorpe A J, 1990: Frontal instability generated by tropospheric potential vorticity anomalies. Q. J. R. Meteorol. Soc., 116, 525-560.

Joly A and Thorpe A J, 1991: The stability of time-dependent flows: an application to fronts in developing baroclinic waves. J. Atmos. Sci., 48, 163-182.

Jones S C and Thorpe A J, 1992: The three-dimensional nature of "symmetric" instability. Q. J. R. Meteorol. Soc., 118, 227-258.

Knight D J and Hobbs P V, 1988: The mesoscale and microscale structure and organization of clouds and precipitation in mid-latitude cyclones. Part XV: A numerical modelling study of frontogenesis and cold-frontal rainbands. J. Atmos. Sci., 45, 915-930.

Lagouvardos D, Lemaitre Y, and Scialom G, 1993: Dynamical structure of a wide cold-frontal cloudband observed during FRONTS 87. Q. J. R. Meteorol. Soc., 119, 1291-1319.

Malardel S, Joly A, Courbet F, Courtier Ph, 1993: Non-linear evolution of ordinary frontal waves induced by low-level potential vorticity anomalies. Q. J. R. Meteorol. Soc., 119, 681-713.

Matejka, T, Houze R A, and Hobbs, P V, 1980: Microphysics and dynamics of clouds associated with mesoscale rainbands in extratropical cyclones. Q. J. R. Meteorol. Sci., 106, 29-56.

Parker D J and Thorpe A J, 1994: The role of snow sublimation at fronts. Q. J. R. Meteorol. Soc., submitted.

Perrson P O G and Warner T T, 1991: Model generation of spurious gravity waves due to inconsistency of the vertical and horizontal resolution. Mon. Wea. Rev., 119, 917-935.

Redelsperger J-L and Lafore J-P, 1994: Non-hydrostatic simulations of a cold front observed during the FRONTS 87 experiment. Q. J. R. Meteorol. Soc., 120, in press.

Schär C and Davies H C, 1990: An instability of mature cold fronts. J. Atmos. Sci., 47, 929-950.

Thorncroft C D and Hoskins B J, 1990: Frontal cyclogenesis. J. Atmos. Sci., 47, 2317-2336.

Thorpe A J and Clough S A, 1991: Mesoscale dynamics of cold fronts: Structures described by dropsoundings in FRONTS 87. Q. J. R. Meteorol. Soc., 117, 903-941

Thorpe A J and Rotunno R, 1989: Non-linear aspects of symmetric instability. J. Atmos. Sci., 46, 1285-1299.

Thorpe A J, 1994: The contributions of Ernst Kleinschmidt to cyclone research, Bergen conf pre-print volume.

POTENTIAL VORTICITY AND THE ELECTROSTATICS ANALOGY

by

Alan J Thorpe and Craig H Bishop

JCMM, Dept of Meteorology
University of Reading
Reading, England

1. INTRODUCTION

The potential vorticity, $PV = \frac{1}{\rho} \underset{\sim}{\zeta} . \nabla \theta$, is conserved by air parcels moving in an adiabatic frictionless way. The notion of conservation leads to the classic Rossby vortex tube schematic picture. It is worth remembering that PV doesn't have the dimensions of vorticity and in the spirit of Rossby's original formulation one might want to define a quantity V:

$$V = f_0 \left[\frac{PV}{PV_0} - 1 \right]$$

where PV_0 is a standard constant potential vorticity defined in terms of a reference density, static stability, and latitude. Then V could more appropriately be called the "potential" vorticity having the additional factor in its definition of requiring the specification of a location in the atmosphere to which it is referred.

However the PV is not conserved in the presence of diabatic sources and frictional forces. This leads to the existence of PV anomalies which subsequent to their production can behave in a conservative way. Given the existence of PV anomalies then we need a way to interpret the dynamical structure associated with anomalies.

The term "invertibility principle" has beeen coined by Hoskins et al 1985 to describe the process whereby a knowledge of the complete distribution of PV in a given region of the atmosphere along with the potential temperature on the boundaries of the region and a balance condition allows one to determine the flow and temperature in that region. However this is not exactly what is required in the case of considering an anomaly or a collection of anomalies. Then we would like to say how much of the flow and temperature is due only to those anomalies. This process is here referred to as "attribution" which involves the act of ascribing as belonging or appropriate to.

A particular mathematical solution to attribution has been described by Davis 1991 in a process referred to as piecewise PV inversion. A discussion of the concept of attribution is given in Bishop and Thorpe 1994. It proves useful from a theoretical viewpoint when considering attribution to draw a parallel with the theory of electrostatics. This electrostatics analogy for PV gives a very evocative physical picture of attribution relying on the (vector) field induced by local anomalies of PV charge. The remote flow and temperature that can be attributed to a given PV anomaly then expresses an action-at-a-distance concept.

2. THE ELECTROSTATICS ANALOGY

2.1 Background

In Bishop and Thorpe 1994 (hereafter BT) the isomorphism between the quasi-geostrophic potential vorticity and a static electrical charge was described. This gave a convenient picture of a PV anomaly being associated with a field distributed through space; the anomaly being observable as the divergence of the field. Outside the anomaly the field is non-divergent. In this paper we consider the extension of these ideas to the Ertel-Rossby form of the potential vorticity (PV). The PV can of course be written in a form proportional to the divergence of a vector field: $PV = \frac{1}{\rho} \nabla.(\underset{\sim}{\zeta} \theta)$. The vector field in question is the product of the three-dimensional vorticity vector and the potential temperature. The divergence form of the Ertel-Rossby PV is fundamental in that the mass-weighted volume integral of PV only depends on the normal component of the vector field at the boundaries. This property is a familiar one and is, of course, common with the quasi-geostrophic form and

electrical charges and their fields.

Here it will be shown that the field close to a PV anomaly is composed of a linear part plus a non-linear component due to the existence of additional PV charge interpretable in terms of bound charge as introduced by BT. The electrostatics analogy helps to bridge the conceptual gap that exists in interpreting effects due to anomalies of quasi-geostrophic and Ertel-Rossby potential vorticity.

2.2 Ertel-Rossby PV

Scale analyses suggest that on synoptic scales the non-divergent wind is much smaller than the irrotational wind. This suggests that the PV obtained by replacing the full horizontal wind by its non-divergent part in the definition of Ertel PV should be well conserved by synoptic scale motions:

$$(\rho\ \theta_0/g)\ PV = \left[f + \nabla_h^2 \psi \right] \phi_{zz} - \psi_{yz}\,\phi_{yz} - \psi_{xz}\,\phi_{xz} \qquad (1)$$

where ϕ is the geopotential, ψ is the streamfunction for the non-divergent wind $v_\psi = (-\psi_y, \psi_x)$ and θ_0 is a constant potential temperature.

To describe anomalies of PV it is necessary to subtract from the local PV an appropriate reference or background distribution - the whole notion of an anomaly depends on this. This is in accord with Rossby's original definition of PV. Here we define a general zonally-average flow dependent on latitude, y, and height, z. Then the geopotential can be divided into a zonal mean and perturbation: $\phi = \bar{\phi}\ (y, z) + \phi'\ (x, y, z, t)$. The streamfunction is similarly divided into a zonal mean and deviation, $\psi = \bar{\psi} + \psi'$ and

$$\overline{PV} = \frac{f\theta_0}{\rho\ g} \left[(f + \bar{\psi}_{yy})\ \bar{\psi}_{zz} - \bar{\psi}_{yz}^{\,2} \right] \qquad (2)$$

To proceed it is convenient to define a reference potential vorticity, $PV_0 = f\ N_0^2\ \theta_0 / g\rho$, where N_0^2 is a constant value. Equation (1) may then be rewritten in the form:

$$e' = (PV - \overline{PV})\ f\ /\ PV_0$$

Note that e' is conserved by the balanced flow but is not conserved in the presence of ageostrophic motion. For attribution it is important to describe how e' is inverted to find that component of the flow and temperature that can be associated with the PV anomaly. In order to invert e', one must have a relationship between ψ and ϕ'. Such a relationship is provided by the divergence equation. Here we use, for illustration, the simplest balance, namely: $\phi' = f\ \psi$. Then we can write: $e' = e'_L + e'_N$ where:

$$e'_L = \nabla.\left[\frac{N^2}{N_0^2}\psi'_x, \frac{N^2}{N_0^2}\psi'_y - \frac{f}{N_0^2}\bar{\psi}_{yz}\psi'_z, \frac{f\zeta}{N_0^2}\psi'_z - \frac{f}{N_0^2}\bar{\psi}_{yz}\psi'_y \right] \qquad (3)$$

$$e'_N = \frac{f}{N_0^2}\nabla.\left[-\psi'_{xz}\psi'_z, -\psi'_{yz}\psi'_z, \nabla_h^2\psi'\psi'_z \right]$$

where $N^2 = f\,\bar{\psi}_{zz}$, $\zeta = f + \bar{\psi}_{yy}$, and $\bar{\psi}_{yz} = -\bar{u}_z$.

2.3 Dielectric constant

These equations can be couched in terms of a dielectric tensor in the following way. It is convenient to make a transformation to the new vertical coordinate $\tilde{z} = z\ N_0/f$. Then we can write $e' = \tilde{\nabla}\ .\ \underset{\sim}{D}'$, where the vector $\underset{\sim}{D}'$ is defined as:

$$\underset{\sim}{D}' = (\underset{\sim}{\varepsilon}_L + \underset{\sim}{\varepsilon}_N)\ \tilde{\nabla}\ \psi' \quad \text{and}$$

$$\tilde{\nabla} = (\partial/\partial x, \partial/\partial y, \partial/\partial \tilde{z})$$

where $\underset{\sim}{\varepsilon} = \underset{\sim}{\varepsilon}_L + \underset{\sim}{\varepsilon}_N$ is the dielectric tensor with components ε_{ij} with i and j ranging from 1 to 3. The linear and non-linear components have been separated viz: $e'_L = \tilde{\nabla}.(\underset{\sim}{\varepsilon}_L\ \tilde{\nabla}\ \psi')$ and $e'_N = \tilde{\nabla}.(\underset{\sim}{\varepsilon}_N \tilde{\nabla}\psi')$. From inspection of equation (3) the components of the linear part of the dielectric tensor is:

$$\varepsilon_{11} = \varepsilon_{22} = \frac{N^2}{N^2} \qquad \varepsilon_{33} = \frac{\bar{\zeta}}{f}$$

$$\varepsilon_{23} = \varepsilon_{32} = \frac{-\bar{u}_z}{f} \quad \& \quad \text{other comps. zero}$$

The components of the non-linear part are as follows:

$$\varepsilon_{i3} = \frac{\zeta'_{rel}}{f} \quad \& \quad \text{other comps. zero}$$

where $\zeta'_{rel} = (-\psi'_{xz}, -\psi'_{yz}, \nabla_h^2\psi')$ is the relative vorticity due to the anomaly.

It can be seen that the linear part only

depends on the background static stability and vorticity. On the other hand the non-linear part depends on the geopotential itself via the relative vorticity; this is not known until the inversion solution has been obtained.

As discussed in BT the existence of a dielectric constant is, in electrostatics, associated with the existence of bound, or polarized, charge. The definition of the bound PV, as given in BT, is:

$$e'_b = - \bar{\nabla} . ((\underset{\sim}{\varepsilon} - 1) \bar{\nabla} \psi)$$

In the quasi-geostrophic case, as described by BT, the bound PV was due to the equivalent of a vertical polarization (as $\underset{\sim}{\varepsilon} - 1$ is only non-zero in the vertical component). It can be seen that in the Ertel-Rossby case it is due to a linear contribution with both horizontal and vertical polarization and a new non-linear contribution assocated with $- e'_N$. Therefore the non-linear parts of the Ertel-Rossby PV are, in this electrostatics analogy, components of the bound charge. This is the major finding of this paper. It provides a simple physical link between the quasi-geostrophic and Ertel-Rossby forms of the potential vorticity.

2.4 Physical interpretation

The interpretation of these equations in the case of a single PV anomaly is now considered. Provided that the anomaly is localised, the magnitude of the streamfunction will decrease with distance away from the anomaly. The non-linear terms and hence the bound charge will decrease with distance more rapidly than the linear terms. The sum of the bound charge within a volume containing the free charge is therefore zero following the divergence form of the bound charge. Thus, from a sufficiently distant vantage point, the total charge density associated with the free charge is equal to the free charge itself.

This representation suggests that e'_L, e' and e'_N are analagous to the total charge density, the free charge density and the bound charge density, respectively. In electrostatics the bound charge arises due to the polarisation of molecules and atoms by an applied electric field. The free charge is that part of the charge field that can be moved around within the medium while it is the total charge that creates field. The field which a point of total charge creates is simply the "free space" Greens function corresponding to the operator defining e'_L. For an infinite atmosphere of uniform N^2 and a suitably stretched vertical coordinate this Greens function would be proportional to the inverse of the distance from the point charge.

3. BACKGROUND PV A FUNCTION OF HEIGHT

A simplification to the general theory described in the previous section is provided by assuming a background PV which is only a function of height. Then there is a background potential vorticity $\overline{PV} = f N^2 \theta_0 / g\rho$, where N is the background Brunt-Vaisala frequency which is a function of height only. The only changes to the equations described in the previous section are that: $N^2 = N^2(z)$, $\bar{\zeta} = f$, and $\bar{\psi}_{yz} = 0$. Therefore the dielectric tensor components become:

$$\varepsilon_{11} = \varepsilon_{22} = \frac{N^2}{N_0^2}, \quad \varepsilon_{33} = 1 \quad \& \quad \text{other comps. zero}$$

and the non-linear components are unchanged.

The linear part only depends on the background static stability which is a known function of height. The non-linear part depends on the geopotential itself via the relative vorticity; this is not known until the inversion solution has been obtained.

Compare this dielectric tensor for the Ertel-Rossby PV with that obtained in BT for the quasi-geostrophic PV. Using the same coordinates as above the relevant quasi-geostrophic forms are: $e' = \bar{\nabla} . \underset{\sim}{D}'_Q$ where $\underset{\sim}{D}'_Q = \underset{\sim}{\varepsilon} \bar{\nabla} \psi'$ and the quasi-geostrophic dielectric tensor only has a linear part with components given by:

$$\varepsilon_{11} = \varepsilon_{22} = 1, \quad \varepsilon_{33} = \frac{N_0^2}{N^2} \quad \& \text{ other comps. zero}$$

It is clear from these expressions for the dielectric constant that the quasi-geostrophic PV is not, in general, equal to the linear part of the Ertel-Rossby PV. They only become equal in the case when there is no vertical variation in the background static stability so that we may define $N^2 = N_0^2$. This has important implications concerning the role of the tropopause.

4. ANALYTICAL SOLUTIONS FOR UNIFORM $\overline{PV}$

In this section the case of a single PV anomaly embedded in a uniform background PV is considered as it provides analytical solutions which make the previous theoretical formulation explicit. For this situation we can take $N_0^2 = \overline{N^2}$ and $PV_0 = \overline{PV}$ as constants. An important simplification arises if the PV anomaly is spherically symmetric in the radial coordinate:

$$r = \left(x^2 + y^2 + \frac{N^2}{f^2} z^2 \right)^{1/2}$$

then the potential, ϕ', also exhibits this radial symmetry.

4.1 Quasi-geostrophic case

The quasi-geostrophic PV can be expressed, using the radial coordinate transformation, as:

$$q' = \frac{1}{f\, r^2} \left(r^2 \phi'_r \right)_r$$

This shows that the quasi-geostrophic PV is, in this case, equivalent to the linear part of the Ertel-Rossby PV e'_L. The magnitude of the anomalies are equal if $q' = e' = (PV - \overline{PV})\, f \,/\, \overline{PV}$.

A simple example of such a PV anomaly is a "ball" which has a constant but different PV compared to the rest of the atmosphere:

$$r > b \qquad q' = 0 \qquad \Rightarrow \phi' = -\frac{f}{3} \tilde{q} \frac{b^3}{r}$$

$$r < b \qquad q' = \tilde{q} \qquad \Rightarrow \phi' = -f \tilde{q} \left[\frac{b^2}{2} - \frac{r^2}{6} \right]$$

4.2 Semi-geostrophic PV

An estimate of the Ertel-Rossby PV is given by the so-called semi-geostrophic potential vorticity, SPV, defined as:

$$SPV = \frac{1}{\rho} \underline{\zeta}_{SG} \cdot \nabla \theta = \frac{1}{\rho} \nabla \cdot (\theta \underline{\zeta}_{SG})$$

$$\text{where} \quad \underline{\zeta}_{SG} = \underline{\zeta}_G + \frac{1}{f_0} \underline{J}_{xyz}(u, v)$$

Following Shutts and Cullen 1987 one can introduce a new potential function, $P = \phi + \frac{f^2}{2} (x^2 + y^2)$, which has the property that $\underline{\zeta}_{SG} = \frac{1}{f^3} \nabla P_x \times \nabla P_y$. Then the SPV can be written as the determinant of a matrix:

$$SPV = \frac{\theta_0}{\rho g f^3} \det \begin{bmatrix} P_{xx} & P_{xy} & P_{xz} \\ P_{yx} & P_{yy} & P_{yz} \\ P_{zx} & P_{zy} & P_{zz} \end{bmatrix}$$

Using a decomposition into a background mean state with uniform potential vorticity and a local deviation, denoted by a prime, then $s' = (SPV - \overline{SPV})\, f / \overline{SPV}$. The SPV has a spherically symmetric form for a spherical PV anomaly field using the radial coordinate. In spherical polar coordinates the SPV can be written as the sum of three parts:

$$s' = \frac{1}{f\, r^2} \left(r^2 \phi'_r + \frac{1}{f^2} r \phi'^2_r + \frac{1}{f^4} \frac{\phi'^3_r}{3} \right)_r$$

It can be shown that the solution of this equation for a localized ball of SPV with $s' = \tilde{s}$ for $r < b$ and $s' = 0$ for $r > b$ is given by the following:

$$\phi'_r = f^2 r \left(\left(1 + \frac{\tilde{s}}{f} \frac{b^3}{r^3} \right)^{1/3} - 1 \right) \quad \text{for } r > b$$

$$\phi'_r = f^2 r \left(\left(1 + \frac{\tilde{s}}{f} \right)^{1/3} - 1 \right) \quad \text{for } r < b$$

These solutions are related to those first given by Shutts 1991 for the total flow including a point anomaly.

In figure 1 the semi-geostrophic and quasi-geostrophic solutions are compared for the case when $s' = q' = 4\, f$. This strong positive anomaly exhibits the important feature that the quasi-geostrophic solution involves local regions of static instability and so is outside its domain of validity. In contrast the semi-geostrophic solution does not exhibit static instability for any magnitude anomaly. It can be seen that inside the anomaly the QG solution has much larger static stability and hence vorticity than its semi-geostrophic counterpart. This is due to the fact that the QGPV is additive in terms of vorticity and stability whereas the SPV is multiplicative.

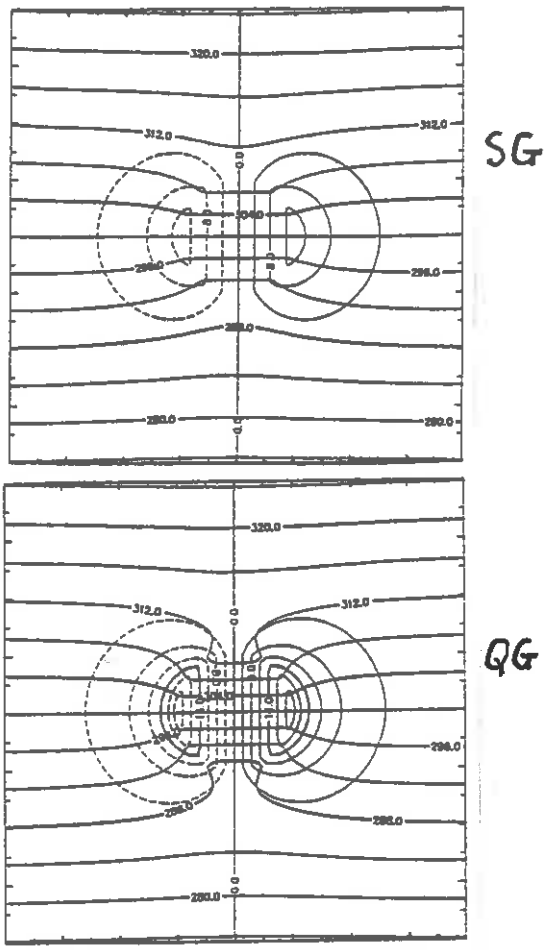

Figure 1: A vertical section showing the isentropes and flow, into the page, for a "spherical" PV anomaly using the QG and SG potential vorticity; $\tilde{s}/f = 4$.

4.4 Semi-geostrophic dielectric constant

Using the terminology of BT the semi-geostrophic PV anomaly can be written in the following form: $\nabla \cdot \underline{D}'_s = s'$. The vector field associated with a semi-geostrophic PV anomaly written in the spherical coordinates is $\underline{D}'_s = \epsilon_s \psi'_r \hat{\underline{r}}$ where $\hat{\underline{r}}$ is a unit vector in the radial direction. The quantity ϵ_s is the semi-geostrophic dielectric constant and has the following form:

$$\epsilon_s = 1 + \frac{\psi'_r}{f\, r} + \frac{1}{3}\left[\frac{\psi'_r}{f\, r}\right]^2$$

It is clear that the SG dielectric constant is not unity even in the case being considered here in which the background static stability is uniform. Therefore the SG potential vorticity exhibits an additional polarizability not present in the QG theory. Furthermore the SG diectric constant depends on the field itself and so is non-linear in character. To complete the electrostatics analogy, as discussed in BT, then the equivalent of the electric and polarization fields can be defined as follows:

$$\nabla \cdot \underline{E}'_s = s' + s'_b \quad \text{and} \quad \underline{E}'_s = \psi'_r \hat{\underline{r}}$$

$$\nabla \cdot \underline{P}'_s = -s'_b \quad \text{and} \quad \underline{P}'_s = \chi_s \psi'_r \hat{\underline{r}}$$

where $\chi_s = \epsilon_s - 1$ and s'_b is the semi-geostrophic bound charge. It is interesting that in quantum electric field theory there is an equivalent to this SG bound charge which is referred to as a vacuum polarization. It is associated with the polarization of the vacuum by the long-range Coulomb field. It is only significant at close range to an electrical charge.

Using the analytical solution allows an explicit expression for the SG dielectric constant to be derived. In figure 2(a) the dependence of ϵ_s on $\tilde{s}$ for $r < b$ is given. Note that the susceptibility, χ_s, has the same sign as the normalised PV anomaly, $\tilde{s}$. In figure 2(b) the radial dependence of ϵ_s shows it rapidly diminishes away from the PV anomaly.

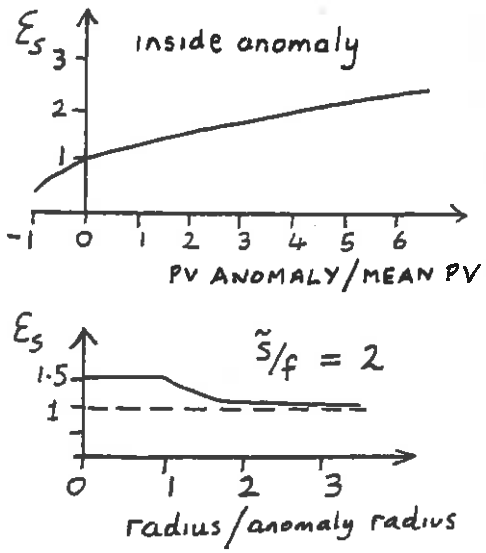

Figure 2: (a) The dependence of the SG "dielectric" constant, ϵ_s, on the PV anomaly strength, $\tilde{s}$, for the region inside the anomaly. (b) The radial dependence of ϵ_s for $\tilde{s} = 2$ f.

As pointed out in BT each element of charge, be it free or bound, has an associated field $\underline{E}'_s$ which is the gradient of a geopotential that is, for a point charge, proportional to $1/\tilde{r}$, where $\tilde{r} = (x^2 + y^2 + z^2)^{1/2}$. This field does not depend on the background potential vorticity and is, of course, linear.

The bound charge, s'_b, can also be evaluated from the ball solution. It can be seen that s'_b is negative inside the ball and positive outside the ball. Notice that these signs are independent of the sign of the PV anomaly, $\tilde{s}$, itself. It is straightforward to prove that the volume integral of this additional PV anomaly, s'_b, is zero. This bound charge, s'_b, is therefore composed of a central negative PV anomaly surrounded by an equal amount of positive PV. It is convenient to visualise this bound charge as due to a polarization process acting in the absence of variations in background static stability. Furthermore this "vacuum" polarization is independent of the sign of the SPV anomaly.

It is illuminating to consider the differences between the QG and SG solutions given in figure 3 for the case described by figure 1. It can seen that the difference is essentially similar to that due to a negative anomaly located within the semi-geostrophic ball charge as can be seen by the anticyclonic flow and temperature dipole. This is consistent with the bound charge being negative in this case.

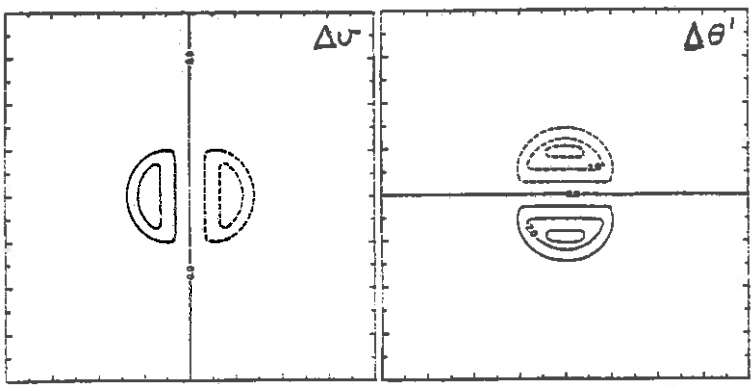

Figure 3: The difference between the solutions, given in figure 1, for a ball of SG potential vorticity and that for a QG anomaly.

6. CONCLUDING REMARKS

In this paper we have shown that the same electrostatics analogy applies to the Ertel-Rossby potential vorticity as for the quasi-geostrophic approximation to potential vorticity. For a PV anomaly embedded in an arbitrary zonally-averaged flow, with background PV varying with latitude and height, the analogy consists of describing the atmosphere in terms of a non-linear dielectric medium. The associated dielectric "constant" is composed of a linear and a non-linear part.

The non-linear contributions are interpreted here as being associated with bound charge. The conceptual simplicity of an element of total (i.e. the linear part) PV charge inducing simple fields, such as that inversely dependant on distance from the anomaly; is then retained. The bound (i.e. non-linear part) PV charge is then caused by the "polarization" of the medium by the field due to the total charge. It acts to modify the simple field only locally to the PV anomaly. In the far-field the bound charge contribution is negligible. This is why many of the essential characteristics associated with a PV anomaly are unchanged from the QG solution.

References:

Bishop C H and Thorpe A J, 1994: Potential vorticity and the electrostatics analogy: quasi-geostrophic theory. Q. J. R. Meteorol. Soc., 120, April issue

Davis C, 1990: Piecewise potential vorticity inversion. J. Atmos. Sci., 49, 1397-1411.

Hoskins B J , McIntyre M E, and Robertson A W: 1985: The use and significance of isentropic potential vorticity maps. Q. J. R. Meteorol. Soc., 111, 877-946.

Shutts G J, 1991: Some exact solutions to the semi-geostrophic equations for uniform potential vorticity flows. Geophys. Astrophys. Fluid Dynamics, 57, 99-114.

Shutts and Cullen, 1987: Parcel stability and its relation to semi-geostrophic theory. J. Atmos. Sci., 44, 1318-1330.

OBSERVATION AND MODELLING OF THE AGGREGATION PROCESS IN A FRONTAL RAINBAND: THE 21st OF JUNE CASE STUDY.

Virginie MARECAL, Anthony J. ILLINGWORTH and Susan P. BALLARD

University of Reading - UK Met. Office,
Reading, United Kingdom

1. INTRODUCTION

Frontal precipitation is usually organised on the mesoscale into rainbands of different types (Hobbs, 1978). Warm frontal rainbands (WFRs) are about 50-100 km wide, oriented parallel to the warm front, located ahead or at the surface warm front and associated with aloft tropospheric vertical motions. In the past, several WFRs have been studied using radiosoundings, radar observations and aircraft mesurements (e.g. Browning and Harrold 1969, Locatelli and Hobbs 1987). It appears that above the warm frontal zone, a shallow layer of potentially unstable air is usually observed and tends to generate active convective cells (called generating cells). The small ice crystals initiated by the generating cells aloft grow by vapour deposition and mainly by aggregation while falling into the stratiform cloud layer below (Hobbs and Locatelli 1978, Herzegh and Hobbs 1980, Matejka et al. 1980). This mechanism leads to a noticible precipitation enhancement at ground level on the mesoscale. Aggregation is thus a dominant process in precipitation formation whithin WFRs. It has to be well evaluated in models in order to get a good precipitation forecast and it is generally poorly represented.

A warm frontal rainband passed over England on the morning of the 21 June 1990. It has been simultaneously sampled by the Chilbolton radar and the Met. Office C130 aircraft. These measurements clearly show that aggregation is very active in precipitation generation. In parallel, a non-hydrostatic mesoscale forecast model (Golding, 1992) is used to simulate this rainband. The microphysical scheme and in particular the aggregation representation has been modified according to the observation in order to better simulate the rainband.

2. OBSERVATIONS

2.1 General situation

On the 21 June 1990, an occluded frontal system passed over the British Isles. A WFR associated with this system has been followed from 0600 UTC by the UK Met. Office FRONTIERS operational radar network. It is about 100 km wide and located ahead and parallel to the warm front and to the occlusion (see Fig. 1). Two reflectivity cores (corresponding to a rainfall rate (RR) of more than 4 mmh^{-1}) are embedded in the rainband.

2.2 Chilbolton radar observations

During the rainband passage, the dual-polarisation Chilbolton radar performed mainly RHI scans (140 km range) at 235° North orientation every 5 minutes on average. The scans were made nearly perpendicular to the rainband (see Fig. 1) and unfortunately did not sample the two precipitation maxima within the rainband. In figure 2 is depicted the reflectivity RHI scan at 1123 UTC. The bright band which corresponds to the melting layer is well defined. This suggests that mainly ice precipitation is present above the 0°C level. The LDR (linear depolarisaton Ratio) and ZDR (differential reflectivity) fields provided by the dual polarisation signals exhibit the signature of the presence of aggregates above the 0°C level. Moreover, the steep gradient in reflectivity in the 500 m above the bright band suggests that aggregation process is active. The rain region located under the bright band in fig. 2 is not uniform with more intense precipitation zones of several

kilometres. This and the wavy pattern that appears aloft might be interpreted as trails of precipitation. This is similar to the reflectivity pattern that can be observed in the presence of generating cells (Browning and Harrold 1969, Herzegh and Hobbs 1980, Locatelli and Hobbs 1987). It is not possible to be fully sure since there are no radar kinematic fields.

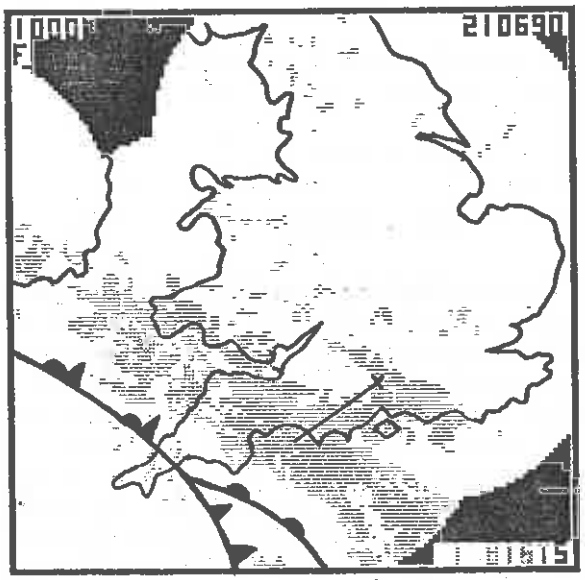

Figure 1: Rainfall rate in mmh^{-1} at ground level at 1000UTC from the Frontiers radar network. The surface fronts are displayed according to the surface observations. The cross shows the Chilbolton radar location and the heavy line corresponds to the trace of the RHI scans. The legend is at the bottom of the figure (< 1, > 1, > 4, > 8 and > 16 mmh^{-1}).

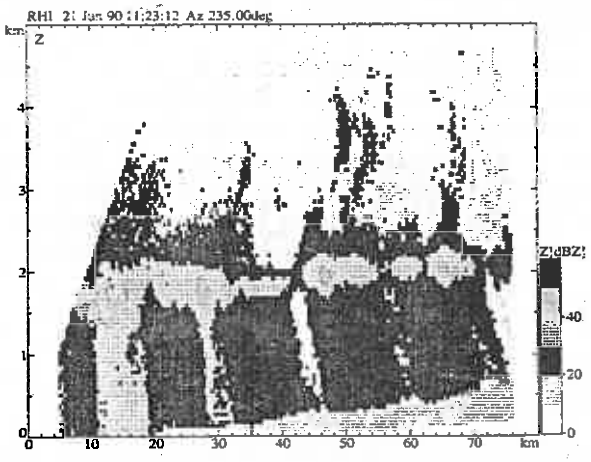

Figure 2: Chilbolton RHI scan at 235° North at 1123 UTC.

2.3 Aircraft microphysical measurements

Aircraft measurements were performed nearby and within the Chilbolton RHI scans plane between 0950 UTC and 1211 UTC by the Met. Office C130 aircraft. The aircraft legs were done between the -2°C and +2°C levels (2.1 to 1.3 km height above ground level). This sampled layer is interesting since the maximum precipitation growth seems to occur just above the 0°C level (see fig. 2). The following microphysical probes were mounted on board the aircraft: a FSSP, a 2DC and a 2DP Knollenberg image probes.

The qualitative analysis of the 2DC and the 2DP images shows that in the 0°C to -2°C layer, large particles recorded are mainly rimed aggregates. Riming is consistent with the presence of cloud water recorded by the FSSP: 0.15 gm^{-3} (mean) and 0.35 (max).

The size-distribution $N_i(D)$ of the sampled ice particles follows an exponential form:

$$N_i(D)=N_{0i}\exp(-\lambda_i D) \qquad (1)$$

For each 10s sample, the N_{0i} and λ_i coefficients have been determined by a least square fit.

These values are compared to Passarelli (1978)'s work on aggregation. He constructed an analytical model of aggregation and vapour deposition growth of an exponential size-distribution of ice particles. An important result of this study is that in the case of steady stratiform precipitation, N_{0i} and λ_i will tend to an equilibrium relationship given by $N_{0i}=C\,\lambda_i^3$, where C depends on the updraft velocity, the temperature lapse rate and the snowfall type.

The (N_{0i}, λ_i) couples determined from the ice particles 2DP images have been plotted and fitted using a least-square fit method (fig. 3). The relationship obtained is:

$$N_{0i}=C\,\lambda_i^x \qquad (2)$$

with $C=1.15\ 10^{-3}\ m^{x-4}$, x=2.9 and a good correlation coefficient of 0.95. Relationship (2) is very close to Passarelli (1978)'s model. This suggests that, in the sampled layer, aggregation is one of the major ice growth processes. Riming is probably acting as well (as discussed before). This process does not affect the size-distribution in the the absence of large variations in the collection efficiency with particles size.

3. MODEL DESCRIPTION

3.1 General description

The model used in this study is the latest version of the UK Met. Office mesoscale forecast model. Its characteristics are described in detail in Golding (1992, 1993). It is non-hydrostatic, fully compressible with a semi-implicit time integration and a semi-Lagrangian advection. The model includes a bulk microphysical scheme with a representation of ice processes which has been improved according to the observations.

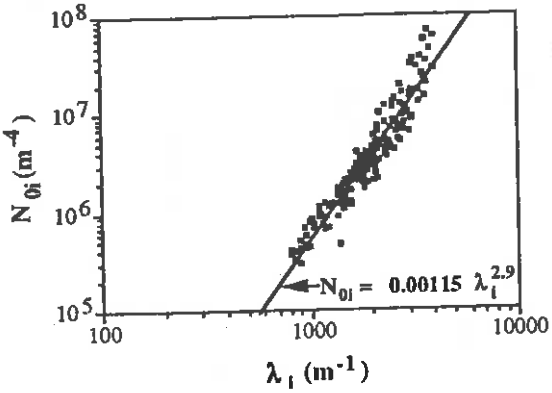

Figure 3: N_{0i} plotted as a fuction of λ_i. The solid line corresponds to the least square fit.

3.2 The improved microphysical scheme

The analysis of the observations (section 2) suggested that riming and aggregation are the dominant processes in the ice precipitation generation within the layer 0°C to -2°C (maximum precipitation growth layer). Riming is a process which is fairly well evaluated in models. On the other hand, aggregation is usually ill-represented. Thus, the problem is : what is the best approach to represent aggregation in the model ?

In models including ice phase processes via a bulk-parameterisation, the ice content (or mixing ratio) is usually divided at least into two categories: cloud ice with a negligible fallspeed and ice precipitation (one or several types) (Cotton et al. 1982, Lin et al. 1983, Rutlegde and Hobbs 1983). This approach allows to take into account the fact that precipitation type and thus precipitation characteristics usually vary with the size of particles due to different initiation and growth processes. Ice precipitation is usually assumed to follow an exponential form with a constant N_{0i}. Ice aggregation is represented by two mechanisms: the autoconversion of cloud ice into precipitation and the accretion of cloud ice by ice precipitation. The autoconversion parameterisation is very ill-controled.

We have chosen to use a different approach. Here, the basic idea is to represent all ice crystals by only one variable: q_i, the mixing ratio of ice. Since q_i includes both small and large particles, q_i is not modified by the aggregation process which is an ice particle-ice particle interaction. Thus, aggregation does not have to be represented in the model by an ill-controled parameterisation. Our approach is physically correct only :

- if one can assume that the simulated rainband contains one very dominant type of ice particles and
- if the model is able to well represent the characteristics of all ice crystals. In other terms, it means that the size-distribution, the mass-dimension and the fallspeed-dimension relationships chosen in the model have to be valid for all particles sizes.

The analysis of the 2D probes aircraft data supports this approach. The sampled particles are, for a very large majority, rimed aggregates as shown by the 2DC and 2DP probes images. The assumption of one type of particles is thus realistic. Moreover, all the particles follow a continuous exponential shape distribution with a dependence between N_{0i} and λ_i given by (2). This represents the aggregation effect on the ice size-distribution. Consequently, the microhpysical scheme of the model has been modified and now includes the observed relationship (2). The problem of using the aircraft data is the representativeness. The aircraft probes sampled a small area with respect to the horizontal dimension of the rainband and a the shallow layer (-2° to +2° C). On the other hand, this layer is where ice particles growth is maximum according to the Chilbolton radar observations and thus it is the most important in terms of microphysics.

The mass-dimension relationship for ice was determined from the aircraft

measurements. The fallspeed-dimension relationship is from Locatelli and Hobbs (1974).

4. MODEL RESULTS

The model is run with a 15 km horizontal grid-spacing and 16 vertical levels above orography (10, 110, 310, 610, ... 12010 m). The domain is 1320 by 1350 km^2 and covers the British Isles. The model is initialized at 0000UTC (operational mesoscale model forecast). The boundary conditions (every 3 hours) are from fine-mesh model forecast (75 km resolution).

4.1. Reference run results

The reference run has the characteristics described above. In figure 4 is represented the RR at ground level given by the model at 1000 UTC. Note that the domain displayed is smaller than the actual calculation domain and is centered around the rainband location. Compared with the observations (fig. 1), the 1 mmh-1 contour is well simulated by the model and maximum values are close to the observations (14 mmh^{-1} simulated and 16 mmh^{-1} observed). On the other hand, the 4 mmh-1 contour is more extended in the model runs. On average, precipitation at ground level is overestimated. Another difference is the location of the intense precipitation zones within the rainband which is not well predicted by the model. This is probably related to the surface front location which is shifted by about 100 km with respect to the observations (see fig. 4). This seems to be due to an error in the large scale forcing imposed by the boundary conditions.

Figures 5ab represent a vertical cross section perpendicular to the rainband (see fig. 4) of θ_e (equivalent potential temperature) and of 'water' content (rain + ice). The warm frontal zone is well marked (see fig. 5a). A convectively unstable zone is located above the rainband. No radiosounding have been launched in the rainband and thus it is not possible to validate this result. Nevertheless, this feature has been observed in the past (e.g. Browning and Harrold 1969, Locatelli and Hobbs 1987). In fig. 5b, the

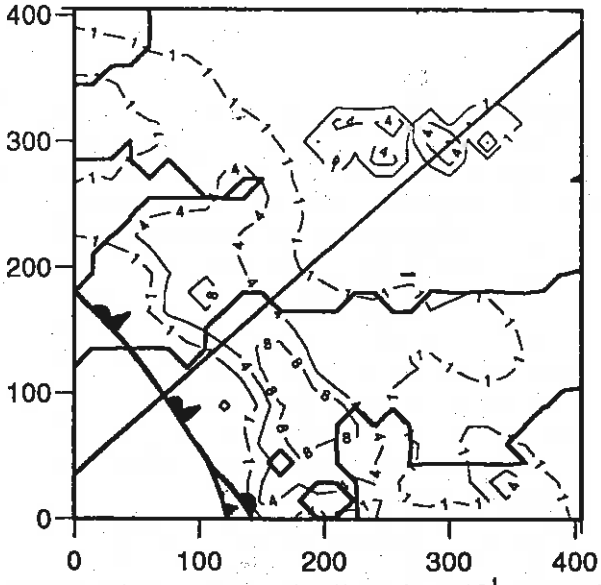

Figure 4: Reference run: rainfall rate in mmh^{-1} at ground level at 1000 UTC simulated by the model. The surface fronts are located according to the model. The solid line gives the location of the vertical cross section displayed in fig 6 and 7. The domain is 405 by 405 km^2.

maximum ice precipitation content is predicted just above the 0°C level as observed by the Chilbolton radar. It is located below the potentially unstable layer. This suggests the presence of generating cells. These cells are of a few kilometres horizontal extension and cannot be resolved by the model which has a 15 km resolution. However, the model simulates an ice precipitation initiation in the unstable layer and an important growth of ice particles while falling. The maximum ice content simulated is similar to that calculated by the aircraft probes (about 0.35 gm^{-3} over a 15 km horizontal distance).

4.2. Sensitivity tests

4.2.1. Cloud ice/precipitation ice scheme

The model was also run with a microphysical scheme including the classic representation of ice and aggregation:

- two variables for ice are solved in the model: cloud ice and ice precipitation,
- ice precipitation size-distribution follows an exponential form with a constant N_{0i}. The N_{0i} value chosen corresponds to the mean N_{0i} recorded by the aircraft 2DP probe,
- autoconversion of ice (aggregation) is represented by the classic

parameterisationgiven by Rutledge and Hobbs (1983).

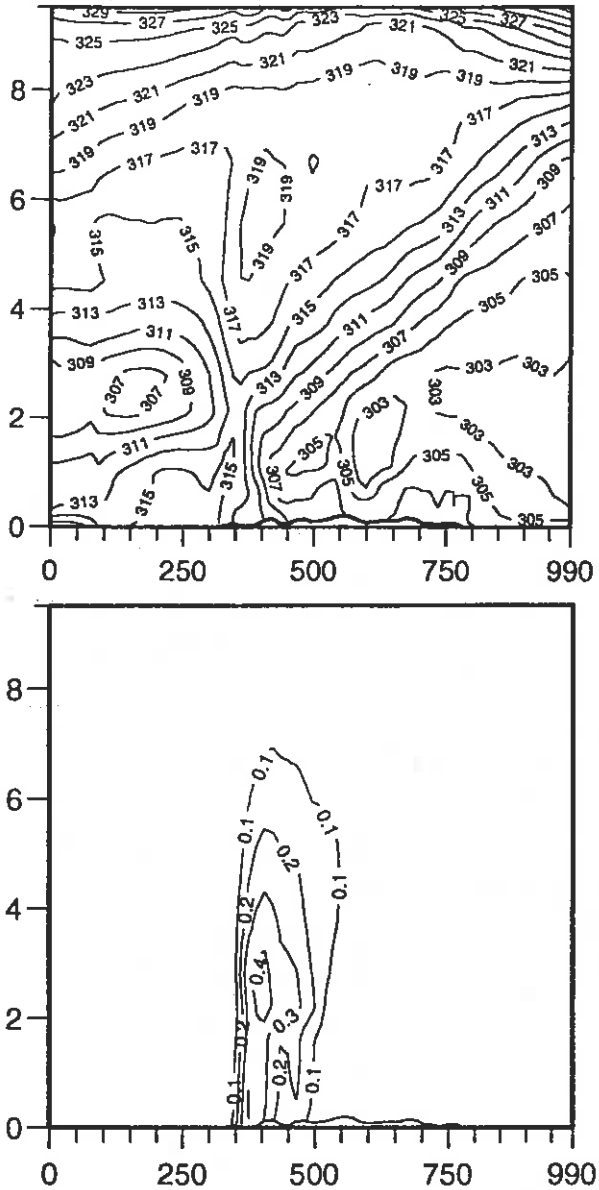

Figure 5: Reference run at 1000 UTC: vertical cross-section perpendicular to the rainband (see fig 4) of (a) θ_e (in K) and (b) precipitation content (in gm^{-3}). The horizontal scale is 990 km.

No important differences with the reference run of the ground level RR can be noted. The reference run gives on average slightly less precipitation. The vertical cross-section of precipitation content is very different in the ice region (fig. 6). The maximum qi for this 'classic' scheme is twice as much as in the reference run and from the aircraft probes. Thus, the reference run gives more realistic results (in terms of ice simulation) even if it overestimates the precipitation content at ground level. Note also that the reference scheme solves at least one equation less and thus is cheaper in terms of computer time.

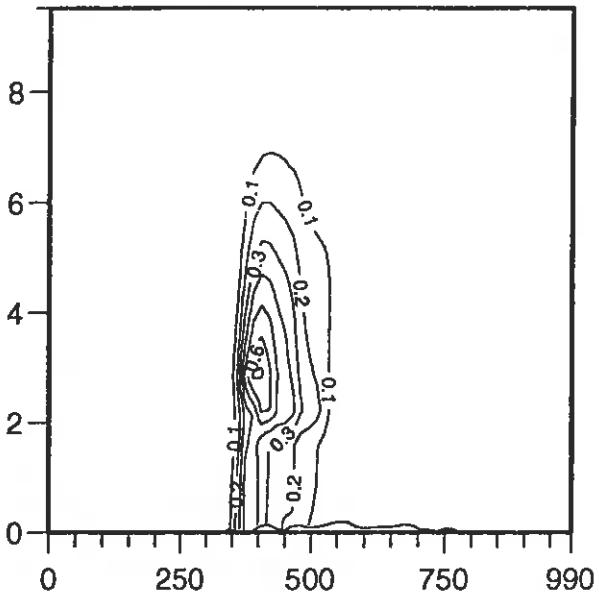

Figure 6: Run with a classic parameterisation (see text): Rainfall rate at ground level (in mmh^{-1}) at 1000UTC. The hosizontal scale is 990 km.

4.2.2 Run with 5km horizontal resolution

The model was run with 5 km horizontal grid-spacing on a limited area domain located around Chilbolton location (405x405 km^2). The model is initialised at 0000 UTC as for the reference run. Boundary conditions are from the reference run.

The ground level RR (fig. 7a) found is much more realistic than the 15 km run. Within the 1 mm h^{-1} contour, a 50 km wide precipitation core is simulated. It is very similar to the main core observed by the Frontiers radars (South of Wales). The maximum values predicted by the model are 14 mmh^{-1} which is very close to the observed values. The core location is about 100 km too far South East with respect to the observations. This location difference is probably due (as for the 15 km run) to a large scale forcing error (via the boundary conditions). In fig. 7b is displayed a vertical cross section parallel to the Chilbolton RHI but shifted by 100 km South East (to take into account the simulation shift with respect to reality). The rain content at ground level is very similar to that recorded

by a disdrometer located nearby Chilbolton. In the ice region, the ice content aloft is consistent with the Chilbolton observations. On the other hand, the maximum ice content is lower (0.2 gm^{-3}) than that recorded by the aircraft.

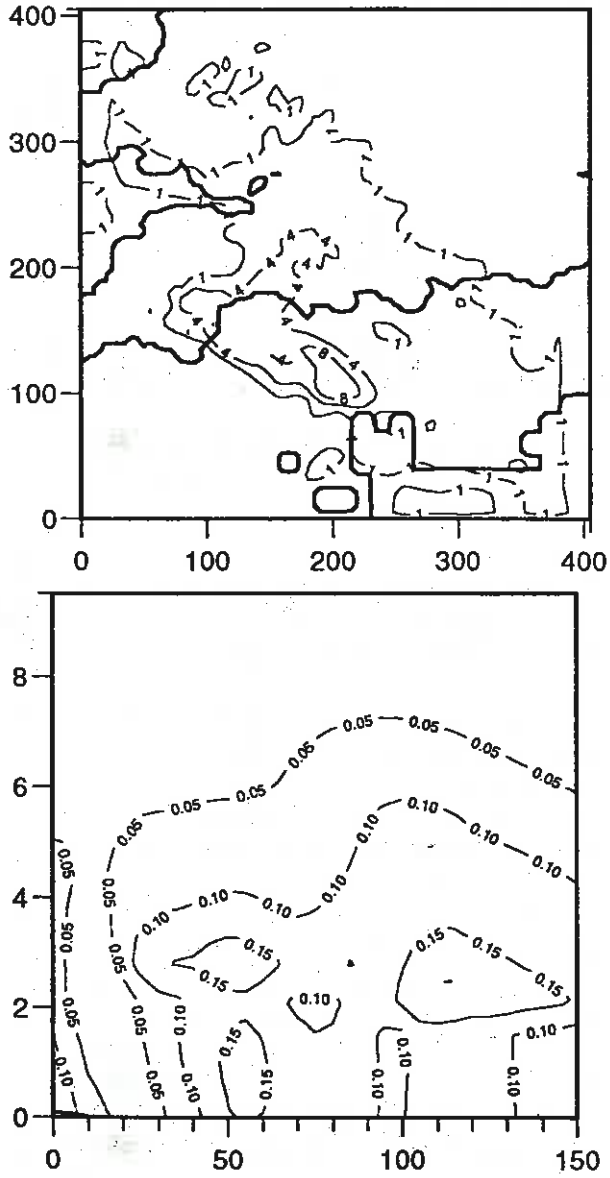

Figure 7: 5 km run at 1000UTC: (a) rainfall rate at ground level in mmh^{-1} and (b) vertical cross section perpendicular to the rainband of water content in gm^{-3} (see text): 150 km horizontal scale.

5 CONCLUSION

The radar and aircraft measurements have shown that ice precipitation within the WFR is mainly created by riming and aggregation just above the 0°C level. They fit well Passarelli's (1978) theory of aggregation and are consistent with previous observational studies.

The microphysical scheme of a mesoscale forecast model has been modified according to the observations results. The major results are:

- precipitation seems to be initiated aloft in a potentially unstable layer,
- the reference run overestimates the overall precipitation at ground level,
- the reference run new scheme gives better results in the ice region than a classic microphysical scheme,
- the 5 km horizontal resolution run gives far better results than the 15 km run.

This work shows that the precipitation simulation, in particular in WFRs, can be improved by introducing measured parameters in the microphysical scheme. The combined use of observations and a model is a good approach to understand the microphysics.

REFERENCES

Browning, K.A., and T.W. Harrold, 1969: Air motion and precipitation growth at a wave depression. *Quart. J. Roy. Meteor. Soc.*, 95, 288-309.

Cotton, W.R., M.A. Stephens, T. Nehrkorn and G.J. Tripoli, 1982 : The Colorado State University three-dimensional cloud/mesoscale model. Part II: An ice phase parameterization. *J. Rech. Atmos.*, 16, 295 - 320.

Golding, B.W., 1992: An efficient non-hydrostatic forecast model. *Meteorol. Atmos. Phys.*, 50, 89-103.

Golding, B.W., 1993: A numerical investigation of tropical island thunderstorms. *Mon. Wea. Rev.*, 121, 1417-1433.

Herzegh, P.H. and P.V. Hobbs, 1980: The mesoscale and micropscale structure and organization of clouds and precipitation in Midlatitude cyclones. II: Warm-frontal clouds. *J. Atmos. Sci.*, 37, 597-611.

Hobbs, P.V., and J.D. Locatelli, 1978: Rainbands, precipitation cores and generating cells in a cyclonic storm. *J. Atmos. Sci.*, 35, 230,241.

Locatelli, J.D. et P.V. Hobbs, 1974: Fallspeeds and masses of solid precipitation particles. *J. Geophys. Res.*, 79, 2185 -2197.

Locatelli, J.D. and P.V. Hobbs, 1987: The mesoscale and microscale structure and organization of clouds and precipitation in midlatitude cyclones.

Matejka, T.J., R.A. Houze Jr and P.V. Hobbs, 1980: Microphysics and dynamics of clouds associated with mesoscale rainbands in extratropical cyclones. *Quart. J. Roy. Meteor. Soc.*, 106, 29-56.

Passarelli, R.E., 1978: An approximate analytical model of the vapor deposition and aggregation growth of snowflakes. *J. Atmos. Sci.*, 35, 118-124.

Rutledge, S.A., and P.V. Hobbs, 1983: The mesoscale and microscale structure and organization of clouds and precipitation in midlatitude cyclones. Part VII: A model for the "seeder-feeder" process in warm-frontal rainbands. *J. Atmos. Sci.*, 40, 1185-1206.

CURRENT JCMM INTERNAL REPORTS

This series of JCMM Internal Reports, initiated in 1993, contains unpublished reports and also versions of articles submitted for publication. The complete set of Internal Reports is available from the National Meteorological Library on loan, if required.

1. **Research Strategy and Programme**
   K A Browning et al
   January 1993

2. **The GEWEX Cloud System Study (GCSS)**
   GEWEX Cloud System Science Team
   January 1993

3. **Evolution of a mesoscale upper tropospheric vorticity maximum and comma cloud from a cloud-free two dimensional potential vorticity anomaly**
   K A Browning
   January 1993

4. **The Global Energy and Water Cycle**
   K A Browning
   July 1993

5. **Structure of a midlatitude cyclone before occlusion**
   K A Browning and N Roberts
   July 1993

6. **Development in Systems and Tools for Weather Forecasting**
   K A Browning and G Szejwach
   July 1993

7. **Diagnostic study of a narrow cold frontal rainband and severe winds associated with a stratospheric intrusion**
   K A Browning and R Reynolds
   August 1993

8. **Survey of perceived priority issues in the parametrizations of cloud-related processes in GCMs**
   K A Browning
   September 1993

9. **The Effect of Rain on Longwave Radiation**
   I Dharssi
   September 1993

10. **Physical Cloud Microprocesses - A Description of the Parametrization used in the Large Eddy Model**
    H Swann
    July 1994

11. **An Appreciation of the Meteorological Research of Ernst Kleinschmidt**
    A J Thorpe
    May 1992

12. **Potential Vorticity of Flow Along the Alps**
    A J Thorpe, H Volkert and Dietrich Heimann
    August 1992

13. **The Representation of Fronts**
A J Thorpe
January 1993

14. **A Parametrization Scheme for Symmetric Instability: Test for an Idealised Flow**
C S Chan and A J Thorpe
February 1993

15. **The Fronts 92 Experiment: a Quicklook Atlas**
Edited by T D Hewson
November 1993

16. **Frontal wave stability during moist deformation frontogenesis**
Part 1. Linear wave dynamics
C H Bishop and A J Thorpe
May 1993

17. **Frontal wave stability during moist deformation frontogenesis**
Part 2. The suppression of non-linear wave development
C H Bishop and A J Thorpe
May 1993

18. **Gravity waves in sheared ducts**
C Bishop and A J Thorpe
November 1993

19. **Potential Vorticity and the Electrostatics Analogy: Quasi-Geostrophic Theory**
C Bishop and A J Thorpe
November 1993

20. **Recent Advances in the Measurement of Precipitation by Radar**
A J Illingworth
April 1993

21. **Micro-Physique et Givrage. Cloud Microphysics and Aircraft Icing**
A J Illingworth
May 1993

22. **Differential Phase Measurements of Precipitation**
M Blackman and A J Illingworth
May 1993

23. **Estimation of Effective Radius of Cloud Particles from the Radar Reflectivity**
N I Fox and A J Illingworth
May 1993

24. **A Simple Method of Dopplerising a Pulsed Magnetron Radar**
A Hau, A J Illingworth and J Eastment
November 1993

25. **Radiation and Polar Lows**
George C Craig
February 1994

26. **Collected preprints submitted to the International Symposium on the Life Cycles of Extratropical Cyclones; Bergen, Norway, 27 June - 1 July 1994**
April 1994

Met Office Joint Centre for Mesoscale Meteorology Department of Meteorology
University of Reading PO Box 243 Reading RG6 6BB United Kingdom
Tel: +44 (0)118 378 8425 Fax: +44 (0)118 378 8791
www.metoffice.com